On the presence of high nitrite (NO_2^-) in coarse particles at Mt. Qomolangma

Zhongyi Zhang[1, 2], Chunxiang Ye[3], Yichao Wu[1], Tao Zhou[4], Pengfei Chen[5,6], Shichang Kang[5,6], Chong Zhang[3], Zhuang Jiang[1], Lei Geng[1, 2, 4*]

[1]Deep Space Exploration Laboratory/School of Earth and Space Sciences, University of Science and Technology of China, Hefei 230026, Anhui, China

[2]CAS Center for Excellence in Comparative Planetology, University of Science and Technology of China, Hefei 230026, Anhui, China

[3]SKL-ESPC & SEPKL-AERM, College of Environmental Sciences and Engineering, and Center for Environment and Science, Peking University, Beijing 100871, China

[4]National Key Laboratory of Deep Space Exploration, Hefei, 230088, Anhui, China.

[5]Key Laboratory of Cryospheric Science and Frozen Soil Engineering, Northwest Institute of Eco-Environment and Resources, Chinese Academy of Sciences; Lanzhou, 730000, Gansu, China

[6]University of Chinese Academy of Sciences; Beijing, 100049, China

* *Correspondence to*: Lei Geng (Email: genglei@ustc.edu.cn; Tel: +86-0551-63600015)

Abstract

Atmospheric reactive nitrogen cycling ~~is crucial for maintaining the atmospheric oxidation capacity of background atmosphere on the Tibetan Plateau~~, with nitrous acid (HONO) and particulate nitrite (NO_2^-) as important intermediates, is crucial for maintaining the atmospheric oxidation capacity of background atmosphere on the Tibetan Plateau. During an eleven-day field campaign at the Base Camp of Mt. Qomolangma in spring of 2022, we observed significant enrichments of NO_2^- in total suspended particulate (TSP) with a mean concentration of 375 ± 386 ng m^{-3}, while NO_2^- was absent in fine particles (PM$_{2.5}$). The comparison revealed that NO_2^- predominately exists in coarse particles. Local surface soil at the sampling site also exhibited high levels of NO_2^-, with δ^{15}N value similar to NO_2^- in TSP. This isotopic similarity suggests that wind-blown soil is probably the primary source of NO_2^- in TSP, accounting for the background levels. While concentration changes of water-soluble inorganic ions in TSP and PM$_{2.5}$ in response to shifts in air mass back-trajectories imply that atmospheric pollutants transported from South Asia may further elevate the NO_2^-, the specific mechanisms of long-range transport resulting in NO_2^- accumulation in TSP rather than PM$_{2.5}$ remain unknown and need to be investigated. The elevated levels of TSP NO_2^- may readily participate in atmospheric reactive nitrogen cycling through gas-particle partitioning or photolysis, leading to the production of HONO, OH and NO and thereby influencing oxidation chemistry. Further efforts on the sources and atmospheric chemistry of particulate nitrite are warranted, particularly in the pristine Tibetan Plateau, where even small inputs of NO$_x$ or HONO can disproportionately affect oxidant budgets and reactive nitrogen cycling.
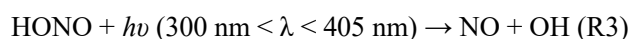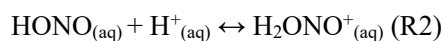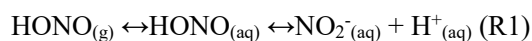
~~Our results reveal an overlooked source of atmospheric NO_2^-, i.e., soil NO_2^-, and highlight in remote regions such as Tibet where other sources are limited, wind-blown soil may serve as an important source of atmospheric NO_2^-. Once lofted into the atmosphere, NO_2^- may readily participate in atmospheric reactive nitrogen cycling through gas-particle partitioning or photolysis, leading to the production of HONO, OH and NO and thereby influencing oxidation chemistry.~~

1 Introduction

The Himalayas-Tibetan Plateau (HTP) represents one of the most important geomorphologically cryospheric regions, boasting high abundance of alpine glaciers and extensive areas of high-altitude snow cover (Kehrwald et al., 2008; Yao et al., 2012; Kang et al., 2019). The melting of snow cover and glacier ice holds immense importance as crucial freshwater resources for over 1.4 billion people in Asia, earning HTP the title as the "Water Tower of Asia" (Immerzeel et al., 2010). However, the enhanced warming rate in the Tibetan Plateau (TP, ~ 0.30°C per decade) has resulted in a rapid and alarming increase in glacier melting over the past decade, significantly affecting the climate, hydrological cycles, and ecosystems at local and global scales (Immerzeel et al., 2010; Xu et al., 2009; Lau et al., 2010). Persistently increased aerosol loadings and greenhouse gas in TP region account for the increased warming rate (Kang et al., 2019; Lau et al., 2010; Lüthi et al., 2015). More importantly, once deposited on the surface of snow cover and glacier ice, the aerosol, especially these light-absorbing components (i.e., black carbon, dust) contribute significantly to the rapid glacial retreat (Xu et al., 2009; Zhao et al., 2020).

Atmospheric oxidation capacity (AOC) regulates ~~the formation of~~ secondary aerosol <u>formation</u> and ~~the removal of~~ trace gases <u>removal,</u> including CH_4 (Wang et al., 2023; Ye et al., 2023; Ye et al., 2016; Andersen et al., 2023), therefore acting as a critical link between atmospheric pollution and cryospheric changes. Previous study have suggested strong solar radiation, high O_3 and relatively high water vapor dominate the relatively strong AOC over the TP (Lin et al., 2008). Recent field campaign further highlighted the rapid reactive nitrogen cycling, with N(III) species (i.e., HONO) as the intermediate, also plays an important role in maintaining the strong AOC in TP (Wang et al., 2023). For example, *Wang et al.* reported high-than-expected HONO (~30 ± 13 pptv) in the Namco station, a typical background site in the middle of TP, with <u>HONO sources including NO_2 heterogenous conversion,</u> soil emission and particulate nitrate photolysis ~~as the dominant sources~~ (Wang et al., 2023). <u>However, a detailed HONO budget analysis indicated these three dominant sources could not account for the observed daytime HONO levels at the background site, implying the existence of additional, yet unidetified, HONO sources. Particulate nitrite likely represents a potential source of HONO through thermodynamic partitioning processes, provided particulate</u>

3

75 <u>nitrite is present in significant amounts under favorable atmospheric conditions</u> (Vandenboer et al.,

76 2014a; Chen et al., 2019; Li, 1994). Interestingly, relatively high levels of nitrite (NO_2^-) in total

77 suspended particulate (TSP) have also been reported from remote sites of TP, i.e., in a forest site in

78 the Southeast Tibet (~ 140 ng m^{-3}) and at the Qomolangma monitoring station (QOMS, ~ 60 ng m^{-}

79 ^{3}) (Bhattarai et al., 2019; Bhattarai et al., 2023). Such high levels of particulate NO_2^- may also

80 contribute to the strong AOC in TP, either via directly photolysis to produce NO_x (Jacobi et al., 2014)

81 or indirectly serve as an important source of HONO through gas-particle partitioning (R1). However,

82 the sources and formation mechanisms for the relatively high level of atmospheric NO_2^- observed

83 in the TP remain unclear.

84 $$HONO_{(g)} \leftrightarrow HONO_{(aq)} \leftrightarrow NO_2^-{}_{(aq)} + H^+{}_{(aq)} \ (R1)$$

85 $$HONO_{(aq)} + H^+{}_{(aq)} \leftrightarrow H_2ONO^+{}_{(aq)} \ (R2)$$

86 $$HONO + h\upsilon \ (300 \ nm < \lambda < 405 \ nm) \rightarrow NO + OH \ (R3)$$

87 The stable nitrogen and oxygen isotopic compositions ($\delta^{15}N$, $\delta^{18}O$, and $\Delta^{17}O$; where $\delta =$

88 ($R_{sample}/R_{reference} - 1$) × 1000‰ and with R denoting the $^{15}N/^{14}N$, $^{18}O/^{16}O$, and $^{17}O/^{16}O$ ratios; $\Delta^{17}O =$

89 $\delta^{17}O - 0.52 \times \delta^{18}O$) may provide diagnostic information regarding the sources and formation

90 pathways of atmospheric nitrite. Similar isotopic approaches have been widely used to explore the

91 nitrate (NO_3^-) sources (Morin et al., 2008; Zong et al., 2020; Geng et al., 2014; Fang et al., 2011;

92 Hastings et al., 2003; Zhang et al., 2022; Zhang et al., 2021b; Liu et al., 2018; Felix and Elliott,

93 2014; Miller et al., 2018). Considering that atmospheric NO_2^- may share similar sources and

94 formation pathways with NO_3^-, the specific NO_2^- formation pathways are expected to be

95 characterized by distinct oxygen or nitrogen isotopic endmembers, despite reports on the

96 atmospheric NO_2^- isotopic compositions are rare. For instance, NO_2^- produced from the photolysis

97 of particulate NO_3^- may possess very negative $\delta^{15}N$ values compared to NO_3^-, analogous to the

98 pronounced nitrogen isotope fractionation effects associated with snow nitrate photolysis (Erbland

99 et al., 2013), while the $\Delta^{17}O$ of NO_2^- is expected to closely resemble that of NO_3^- as the oxygen atom

100 in NO_2^- is imparted from NO_3^-, unless significant oxygen atom exchange between NO_2^- and aerosol

101 water occurs. The $\Delta^{17}O$ of NO_2^- (and HONO) from primary emission sources is expected to be

102 negligible, while that generated from heterogeneous reactions of NO_2 on the aerosol surface would

be characterized by positive $\Delta^{17}O$ values depending on the degree of NO_2^- and aerosol water oxygen isotope exchange. These unique isotopic fingerprints may be utilized in distinguishing the sources and formation pathways of atmospheric NO_2^-.

To gain insight into the sources and/or formation mechanisms of atmospheric NO_2^- in the pristine environment of TP, we collected the TSP and fine particulate matter ($PM_{2.5}$) synchronously at the Base Camp, the north slope of the Mt. Qomolangma during the campaign of "Earth Summit Mission-2022" scientific expedition from April 24th to May 6th, 2022, with additional surface soil samples collected in May, 2023. The NO_2^- concentration and multi-isotopic signatures ($\delta^{15}N$, $\delta^{18}O$, and $\Delta^{17}O$) in aerosol and surface soil were then determined in order to evaluate the potential sources of atmospheric NO_2^-. Additionally, the potential environmental implication of atmospheric nitrite was explored in the term of atmospheric oxidation capacity at this pristine environment.

2 Material and Method

2.1 Site description

The Base Camp is located in the middle of the Rongbuk valley (86.85 °E, 28.14 °N), situated ~5200 m above sea level (m a.s.l) on the north slope of the Mt. Qomolangma (Zou et al., 2008; Zhu et al., 2006). The surrounding surface consists of loosed soil, gravel, broken rocks of various sizes, with sparse vegetation due to the semi-arid status (Ming et al., 2007; Zou et al., 2008). Rongbuk valley is characterized by a depth of ~1000 m and a floor width of ~1000 m, with elevations of the surrounding mountains exceeding 6000 m on both sides (Zou et al., 2008). Attributed to the unique topography, the local air circulation is dominated by mountain and valley breezes. The predominant wind regime is the katabatic flow of southerly and southeasterly, which is typically persists from noon to midnight (Zhu et al., 2006; Zou et al., 2008; Zhou et al., 2011). The nearest accessible area for residents and visitors is at least 2 km north of the Base Camp. During the campaign, electricity and natural gases were routinely used for cooking and hot water production. There were intermittent vehicle exhaust emissions around the station during daytime for the daily necessaries supporting, i.e., water and food. To minimize the influence of local anthropogenic activities on sampling, the instruments were set in the ~~southwest~~ southeast (upwind direction, Figure S1) and approximately 100 m away from the living space of the Base Camp. The anthropogenic

5

131   influence on the sampling is expected to be minimal.

2.2 Field campaign and sample collection

133   From April 26th to May 6th, 2022, TSP samples were collected simultaneously with NO$_2$ using

134   a homemade denuder-filter system (Zhou et al., 2022). A similar system has been widely used to

135   separately collect atmopsheric particulate matter and N-containing gases for isotopic analysis,

136   suggesting the mutual interference between the particulate and gaseous phases to be minimal. A

137   polytetrafluoroethylene (PTFE) sleeve is used to assemble the homemade denuder with the filter

138   pack, flowmeter, and pump. The filter pack was placed in the front of the denuder. All connections

139   between the various parts of the sampling apparatus are made using 3/8″ Teflon tubing. A detailed

140   description of the sampling apparatus can be found in our previous report (Zhou et al., 2022).

141   Whatman quartz filter (circles, diam. 47mm, pre-heated at 400 ℃ for 3 h before use) was placed

142   into the filter pack to collect TSP sample. In the present study, the collected bulk aerosol can be

143   regarded as ~~total suspended particulate~~TSP since no size-selective inlet was employed. The flow

144   rate was controlled at 30 L/min^{-1} using a flowmeter, ~~corresponding to a filter face velocity of~~

145   ~~approximately 0.288 m s^{-1}~~. Previous reports have indicated that the ~~face velocity~~flow rate has

146   negligible effect on the concentrations of sulphate, nitrate, and ammonium when using quartz filter

147   for sampling (Keck and Wittmaack, 2005). To minimize the potential influence of the loose ground

148   surface on the TSP collection, a mountain tent was used to separate the pump (out the tent) with the

149   denuder-filter system (in the other side of tent), and the inlet Teflon tube was stretched out of the

150   tent for ~1.5 m height straight.

151   From April 24th to May 6th, 2022, PM$_{2.5}$ were sampled using a high-volume aerosol sampler

152   (TH-1000F; Wuhan Tianhong Instruments Co. Ltd., China) equipped with PM$_{2.5}$ inlet and Whatman

153   quartz-fiber filters (sheets, 203 mm × 254 mm) at a flow rate of 1.5 m^3/min. All the quartz filters

154   were pre-heated at 400 ℃ for 3 h before use. In general, TSP and PM$_{2.5}$ samples were collected with

155   diurnal resolution during this campaign, with daytime samples from approximately 09:00–20:00

156   and nighttime samples from 21:00–08:00 (local time), respectively. From May 2nd to May 4th, we

157   collected the daytime TSP and PM$_{2.5}$ samples in the morning (09:00-14:00) and afternoon (14:00-

158   20:00), respectively. A total of 24 TSP samples (including 2 blanks) and 29 PM$_{2.5}$ (including 3 blanks)

159   were collected during this campaign. After each sampling period, quartz filters were removed from

160 the filter pack/PM$_{2.5}$ inlet and immediately wrapped in pre-baked aluminum foil and and then stored

161 in frozen until analysis to minimize potential loss of nitrite. During the campaign, snowfall events

162 occurred on the night of April 29th and during the daytime of April 30th.

163   Surface soil samples (0-5 cm depth, n = 9) were collected in May, 2023 from the east slope,

164 west slope and south sides of the Rongbuk valley on both sides of the Rongbuk valley (i.e., east and

165 west) as well as on the south side in May, 2023. A polytetrafluoroethylene (PTFE) shovel was used

166 to collect soil. The collected soil was immediately transferred to clean plastic bags, sealed and kept

167 frozen. Soil samples were transported into laboratory using a cold chain. Upon arrival at our

168 laboratory, the soil samples were passed through a 60-mesh screen (~0.25 mm) to remove larger

169 particles and thoroughly homogenized prior to chemical and isotopic analysis.

2.3 Ionic concentration analysis and uncertainty estimation

171   Water-soluble inorganic ions (WSIs, including Na$^+$, NH$_4^+$, K$^+$, Mg^{2+}, Ca^{2+}, Cl$^-$, NO$_2^-$, NO$_3^-$, and

172 SO$_4^{2-}$) in TSP (entire filter, ~16.6 cm^2) and PM$_{2.5}$ (1/32 section, ~13.0 cm^2) were extracted using 20

173 mL Milli-Q ultrapure water (18.2Ω cm) in an ultrasonic bath at room temperature for 30 min. Note

174 the TSP filters were cut to fit the filter holder from the standard Whatman quartz-fiber filters which

175 were also used as the PM$_{2.5}$ filters. After filtration through a 0.22 μm pore size syringe filter which

176 was pre-cleaned with ultrapure water, the extract filtrate was subjected to inorganic species analysis

177 using ion chromatography (Dionex Aquion) (Zhang et al., 2020). Blank samples filters were

178 pretreated and analyzed measured the same as real samples, and the limits of detection (LOD) was

179 calculated as 3 times of standard deviations of blanks (Fang et al., 2015) along with the aerosol

180 samples. The ionic concentrations reported here were blank corrected (volatile components (i.e.,

181 NH$_4^+$, NO$_2^-$, NO$_3^-$) and K$^+$ in blank are always below the detection limits; SO$_4^{2-}$, Mg^{2+} and Ca^{2+} in

182 blank are generally lower than samples by at least five times (the lower end); Na$^+$ in the blank is

183 comparable to samples and was not presented in this study). The analysis uncertainties were

184 typically within 5% standard deviation based on replicate measurements of standards (n = 10). The

185 detection limit for the inorganic species is general less than 6 ng mL^{-1}. In general, Na$^+$ in the blank

186 filters is comparable to samples, a well-known issue for the Whatman quartz filter which is high in

187 Na$^+$ blank. Therefore, in this study, we discarded the Na$^+$ data. The volatile components (i.e., NH$_4^+$,

188 NO$_2^-$, NO$_3^-$) and K$^+$ in blank are low but several times higher than the detection limits; SO$_4^{2-}$, Mg^{2+}

and Ca^{2+} in blank are significantly higher than the respective LOD but lower than samples by at least five times (the lower end). All reported concentrations of each ion were blank corrected as follows:

$$C_i = \frac{(\rho_{sample} - \rho_{blank}) \times V_{water} \times F}{V_{air}}$$

with C_i representing the ambient concentrations of specie i in air (ng m^{-3} or μg m^{-3}), ρ_{sample} and ρ_{blank} are the concentrations determined by the ion chromatography (ng mL^{-1}), V_{water} is the volume of ultrapure water used for extraction (20 mL), V_{air} is the volume of air sampled for each PM$_{2.5}$ or TSP filter, F is the ratio of particulate matter collection area for PM$_{2.5}$ or TSP filters to the filter area used for extraction.

The overall uncertainty in ion concentration was estimated according to the law of error propagation, accounting for the sampling air volume (3% for PM$_{2.5}$ samples and 1% for TSP samples as provided by the manufactures), the extraction of water volume (~0.3% for pipetting from the manufacture Eppendorf), the blanks, and the analytical uncertainty from ion chromatography and calibration, assuming that these factors are independent. The analytical uncertainty for water-soluble ions concentration determination using ionic chromatography has been extensively assessed in our laboratory, with values typically <5% for all inorganic species at concentration of 500 ng mL^{-1}. The combined uncertainty about the ionic concentrations in PM$_{2.5}$ and TSP are shown in Table S1. In general, TSP samples are associated with relatively high overall uncertainty compared to PM$_{2.5}$ samples, perhaps due to the relatively high blank variability due to the low mass loading in TSP.

For soil ionic concentration analysis, 4.0 g sieved soil was extracted using 20 mL Milli-Q ultrapure water, shaken for 30min at room temperature. After centrifugation, the extract was passed through 0.45 mm filters before ions analysis. The concentration determination of water-soluble inorganic ions in soil extract was similar to that of aerosol samples. Detailed procedure for the extraction of soil inorganic ions, especially the NO$_2^-$ has been descried in previous report (Homyak et al., 2015).

2.4 Isotopic analysis

After concentration measurements, isotopic analyses (δ^{15}N, δ^{18}O, and Δ^{17}O) of NO$_2^-$ in TSP

were conducted using the azide method (Casciotti et al., 2007). The azide method can reduce nitrite ion in solution into N_2O in a single step, while nitrate ion remains unchanged, ensuring no interference on the nitrite isotopic analysis. The azide reagent is prepared by mixing 2 M sodium azide with 40% acetic acid at a 1:1 ratio by volume in our laboratory. NO_2^- standards and samples were pretreated under identical conditions concerning the total volume, nitrite amount, water isotope, and matrix. The $\delta^{15}N$, $\delta^{18}O$, and $\delta^{17}O$ of N_2O reduced from NO_2^- in the TSP samples and standards were determined using a Finnigan® MAT253 plus isotope ratio mass spectrometer (IRMS) equipped with a GasBench II and preconcentration system. The data calibration followed the procedures described in *Albertin et al.*, 2021, using three international KNO_2 salt standards (RSIL-N10219, RSIL-N7373, and RSIL-N23 with respective $\delta^{15}N$ and $\delta^{18}O$ values of 2.8/88.5 ‰, -79.6/4.2 ‰, and 3.7/11.4‰). The $\Delta^{17}O$ values of the three international references have not been certified. To address this, a series laboratory experiments was conducted to determine the true values of three international references in our laboratory (Zhang et al., 2025). In brief, each nitrite international reference was oxidized into NO_3^- by O_3 produced from commercial ozone generator. A parallel flow of O_3 was also used to convert a normal KNO_2 salt ($\Delta^{17}O=0$) into NO_3^- to quantify the $\Delta^{17}O$ transfer during O_3 oxidation, following the approach of ~(Vicars and Savarino, 2014). Based on these experiments, the $\Delta^{17}O$ of RSIL-N7373 and RSIL-N23 are determined to be negligible, consistent with previous findings (Albertin et al., 2021), while the $\Delta^{17}O$ of RSIL-N10219 is determined to be (-9.3 ± 0.2) ‰ in our laboratory~~The $\Delta^{17}O$ of RSIL-N7373 and RSIL-N23 are suggested to be zero (Albertin et al., 2021), while the $\Delta^{17}O$ of RSIL-N10219 is determined to be (-9.3 ± 0.2) ‰ in our laboratory.~~ The ^{17}O-excess in samples is then calculated as $\Delta^{17}O = \delta^{18}O - 0.52 \times \delta^{17}O$. The standard deviations for $\delta^{15}N$, $\delta^{18}O$, $\Delta^{17}O$ of reference materials (n = 10) were determined to be less than 0.1‰, 0.6‰, and 0.4‰, respectively.

For soil NO_2^- isotopic analysis, ~30.0g sieved soil was extracted using 150 mL Milli-Q purewater. The soil extract was then preconcentrated into 10 mL using ion-exchange resin before isotopic analysis. The preconcentration approach was widely used for nitrate isotopic analysis in snow and ice samples, and the detailed procedures and the performance have been provided in *Erbland et al.,* 2013 and evaluated in our laboratory (Text S1). The concentrated soil extracts (50 nmol NO_2^-) was then subjected to soil NO_2^- isotopic analysis by converting into N_2O via the azide

method. The remaining procedures of soil NO_3^- and NO_2^- analysis were same as those for TSP samples, as aforementioned.

2.5 Complementary analyses of air mass backward trajectory

To evaluate the possible impact of biomass burning emissions or other pollution sources from South Asia, the Hybrid Single-Particle Lagrangian Integrated Trajectory (HYSPLIT) model (performed using TrajStat plugin of the MeteoInfo software) and archived Global Data Assimilation System (GDAS) of meteorological data were used to model the air mass back trajectories (Wang, 2014). In this study, six-day air mass backward trajectories with arriving height of 1000 m above ground level were simulated to identify the most likely pathway and potential source regions of the air masses at the Base Camp. Moreover, the Fire Information and Resource Management System (FIRMS) developed by Moderate Resolution Imaging Spectrometer (MODIS) (https://worldview.earthdata.nasa.gov) was employed to identify the distribution of active fire spots during the sampling period.

3   Results

3.1 Mass concentrations of water-soluble inorganic ions in TSP and PM$_{2.5}$

Figure 1 displays the chemical compositions of water-soluble inorganic ions, their corresponding time series and fractional contributions in TSP and PM$_{2.5}$. Throughout the campaign, substantial variations of total WSIs in PM$_{2.5}$ and TSP were observed, with a general decline after May 1st. For PM$_{2.5}$ samples, the mass concentrations of total WSIs before April 30th were higher than that from May 1st to May 6th (4.1 ± 1.7 versus 1.7 ± 0.6 μg m^{-3}; $p < 0.05$). The cut-off date of April 30th was initially selected based on observed shifts in concentrations of water-soluble ions and air mass origins (described in section 4). This decline of total WSIs after April 30th was predominately driven by significant reductions in secondary inorganic species, i.e., SO_4^{2-}, NO_3^- and NH_4^+, with the magnitude by more than 60%. In particular, NH_4^+ in PM$_{2.5}$ declined from was on average (322 ± 243) ng m^{-3} before April 30thMay 1st to negligible after May 1st whereas NH_4^+ in PM$_{2.5}$ collected during daytime and nighttime of May 1st were 1 ng m^{-3} and 3 ng m^{-3}, respectively, and NH_4^+ in PM$_{2.5}$ extractions collected from May 2nd to May 6th was below the detection limit. Therefore, the fractional contribution of secondary inorganic species in PM$_{2.5}$ also decreased (Figure

1d). Similarly, K^+ in $PM_{2.5}$, a good tracer of biomass burning (Ma et al., 2003), also declined significantly after April 30th May 1st (269 ± 432 versus 22 ± 12 ng m^{-3}; $p < 0.05$). The elevated concentrations of WSIs before May 1st (4.1±1.7µg m^{-3}) are comparable to previous reports at remote sites over the TPQOMS station (i.e., Namco, 4.2±2.2 µg m^{-3}QOMS) in the spring (Wang et al., 2020; Lin et al., 2020; Lin et al., 2021; Decesari et al., 2010). In comparison, concentrations of Ca^{2+} and Mg^{2+}, tracers of wind-blown dust (Wang et al., 2002), decreased by less than 20% after May 1stApril 30th, with a smaller degree than secondary species. In general, SO_4^{2-}, NO_3^-, and Ca^{2+} are the most abundant species in $PM_{2.5}$, accounting for the majority of the mass of total WSIs. In addition, despite the average daytime concentrations of the inorganic species were generally higher than those at night, no clear diurnal variation of water-soluble inorganic ions in $PM_{2.5}$ was observed in this study (Figure S2).
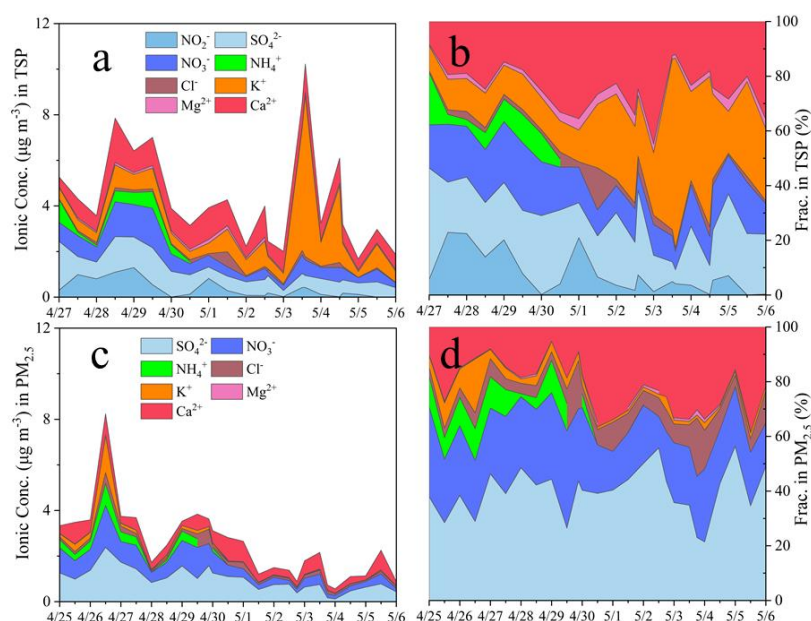

Figure 1. The chemical compositions and time series of mass concentrations of water-soluble inorganic species (NO_2^-, SO_4^{2-}, NO_3^-, Ca^{2+}, etc.), as well as the corresponding mass fractions in respective TSP (a, b) and $PM_{2.5}$ (c, d) samples collected at Base Camp of Mt. Qomolangma in spring 2022.
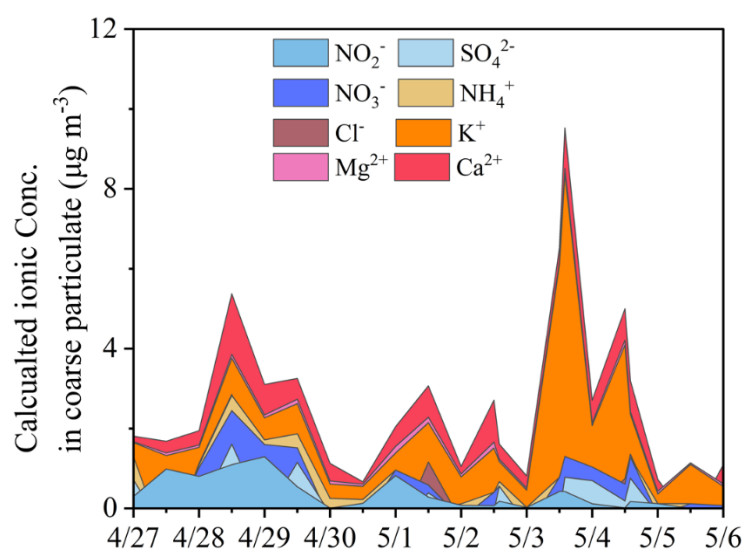
289

Some water-soluble inorganic ions (i.e., SO_4^{2-}, NO_3^- and NH_4^+) in TSP showed similar variation trends with that in $PM_{2.5}$ throughout the campaign, while others, such as K^+, exhibited divergent behavior ~~The variations of WSIs in TSP generally followed a similar pattern to that in PM2.5~~ (Figure 1). For example, after April 30th~~May 1st~~, the secondary inorganic species in TSP declined considerably by over 50% (i.e., NH_4^+ in TSP declined by more than tenfold), while Ca^{2+} in TSP decreased with a smaller degree (< 15%) and Mg^{2+} remained stable. In contrast, TSP K^+ (from both crustal and biomass burning sources)(Hsu et al., 2009) drastically surged on May 3rd and May 4th. Note that other species in TSP, i.e., SO_4^{2-} and NO_3^- also increased to some extent on May 3rd. The time series of water-soluble inorganic ions in the coarse-mode particulate, calculated as the differences between TSP and $PM_{2.5}$, are presented in Figure 2. Due to the overall analytical uncertainties, the air concentrations of SO_4^{2-} in $PM_{2.5}$ samples occasionally exceeded that in corresponding TSP samples on some days.

Figure 3 presents the ion balance of measured water-soluble ions in $PM_{2.5}$ throughout the campaign as well as in TSP collected before and after April 30th, respectively, to highlight the

significant decline in TSP NO_2^-. There is a strong correlation between cation and anion equivalents in $PM_{2.5}$ samples ($R^2 = 0.70$), whereas the correlations decreased in TSP samples ($R^2 = 0.46$ before April 30th and 0.49 after that, respectively). The nanogram-equivalent weight of cation is significantly higher than that of anions for all samples, with ratio of cation to anion equivalent of ~ 1.5 for $PM_{2.5}$, ~1.9 for TSP collected before April 30th, ~4.2 for TSP collected after May 1st. Clearly, the declines in TSP NO_2^- after April 30th results in relatively higher cation/anion equivalent ratio. The slopes of the correlation lines exceed unity for $PM_{2.5}$ and TSP samples, indicating the alkaline nature of aerosol. The observed deficiency of anion can be attributed to the presence of carbonates (i.e., $CaCO_3$), which can dissolve in water during extraction to release CO_3^{2-} and/or HCO_3^- despite the relatively low solubility (Zhang et al., 2021a).

The most distinct feature of chemical compositions in TSP was the elevated level and significant variation of NO_2^-, ranging from 0.2 ng m^{-3} to 1291 ng m^{-3} in air and with an average of 375 ± 386 ng m^{-3}. In comparison, NO_2^- consistently remained below the detection limit in $PM_{2.5}$ samples. Note during the laboratory measurements of ionic concentrations, TSP and $PM_{2.5}$ filters were extracted with ultrapure water and it was the extraction analyzed by ion chromatography. To ensure fair comparisons, similar areas of filters were extracted with same volume of ultrapure water, so that the extractions from the $PM_{2.5}$ filters should be more concentrated in atmospheric particulate species compared to that from the TSP filters, since $PM_{2.5}$ samples were collected at a much faster sampling speed (1.5 m^3 min^{-1} vs. 30 L min^{-1}) over the same sampling duration. Nevertheless, NO_2^- was detectable only in the extractions of TSP filter. The determined NO_2^- concentrations in TSP in this study (375 ± 386 ng m^{-3}) were higher than previous reports conducted in various remote sites, such as at QOMS station (~60 ng m^{-3} for TSP) (Bhattarai et al., 2023), at a forest site in the Southeast Tibet Plateau (~140 ng m^{-3} for TSP) (Bhattarai et al., 2019), in the middle hills of the central Himalayas (~210 ng m^{-3} for TSP) (Tripathee et al., 2021).

In particular, there was a dramatic decrease in TSP NO_2^- after April 30th~~May 1st~~, from a mean of (625 ± 457) ng m^{-3} to (147 ± 145) ng m^{-3}, in line with the declines in other secondary inorganic species. Over the course of the campaign, NO_2^- comprised approximately 8% of the total WSIs mass in TSP, while its contribution reached maximum of ~20% on April 27th and April 28th, being one of the most abundant components on the two days. In addition, there was a strong correlation between

340 NO_2^- and NO_3^- throughout the campaign ($r = 0.75$, $p < 0.05$. Figure ~~S1~~S3). Meanwhile, the mean

341 mass ratio of NO_2^- to NO_3^- was ~50% throughout the campaign, but on several days (i.e., <u>night of</u>

342 April 27th) NO_2^- concentrations significantly exceeded that of NO_3^- <u>(802 vs. 663 ng m^{-3})</u>. Previous

343 study also reported comparable NO_2^- and NO_3^- concentrations in at a forest site in the Southeast

344 Tibet (summer:100 ng m^{-3} vs. 110 ng m^{-3}; winter: 180 ng m^{-3} vs. 270 ng m^{-3}) (Bhattarai et al., 2019).
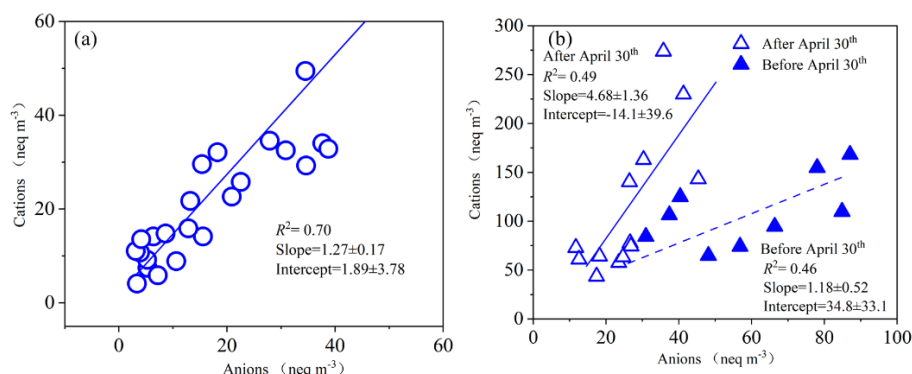

346 **Figure 3.** Ion balance for PM$_{2.5}$ (a, blue circles) and TSP samples (b, blue hollow triangles: samples
347 collected after April 30th; blue solid triangles: samples collected before April 30th). Concentrations
348 are expressed in nanogram-equivalent weight per cubic meter (neq m^{-3}).

3.2 Isotopic signatures of nitrite in TSP

350 Figure ~~2~~4 presents the times series of $\delta^{15}N$, $\delta^{18}O$ and $\Delta^{17}O$ of NO_2^- in TSP, along with the NO_2^-

351 concentrations. Similar to the variation trend of NO_2^- concentrations, NO_2^- isotopes varied in a wider

352 range before <u>April 30th</u>~~May 1st~~, but became more stable afterward. For example, $\delta^{15}N(NO_2^-)$ ranged

353 from -10.9 ‰ to 0.8 ‰, with a relatively large standard deviation before <u>April 30th</u>~~May 1st~~ compared

354 to that after May 1st ((-6.4 ± 4.3) ‰ vs. (-8.0 ± 0.7) ‰). The large variability in $\delta^{15}N(NO_2^-)$ before

355 <u>April 30th</u>~~May 1st~~ is predominately attributed to the two high values observed in daytime of April

356 27th and night of April 28th. Note that the two high $\delta^{15}N(NO_2^-)$ samples were also associated with

357 relatively high NO_2^- mass concentrations ~~but relatively low $\delta^{18}O(NO_2^-)$~~. In contrast to the declining

358 trend of NO_2^- concentrations, the mean $\delta^{15}N(NO_2^-)$ values were comparable before and after <u>April</u>

359 <u>30th</u>~~May 1st~~. Relatively large variability was observed in TSP $\delta^{18}O(NO_2^-)$, ranging from -9.0‰ to

360 3.9‰ and with an average of (-3.4 ± 3.8) ‰. TSP $\Delta^{17}O(NO_2^-)$ varied within a narrow range from -

361 0.2‰ to +0.7‰ and with a mean of (0.2 ± 0.3) ‰. During the campaign, no significant correlations

362 were observed between $\delta^{15}N(NO_2^-)$ and the NO_2^- concentrations; while $\delta^{18}O(NO_2^-)$ appeared to be

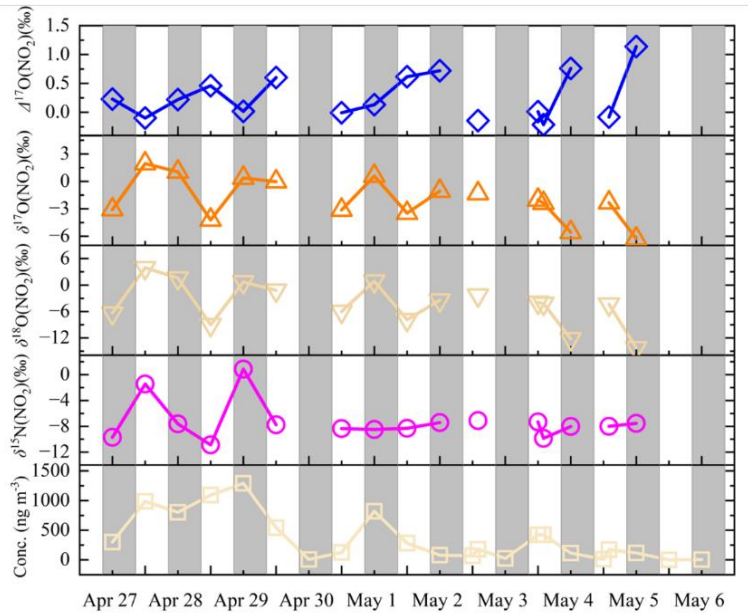363 moderately correlated with the NO_2^- concentrations (Figure ~~S2~~S5).

364

Figure 2~~2~~<ins>4</ins>. Time series of multiple isotopic signatures of NO_2^- ($\delta^{15}N$, $\delta^{18}O$, $\delta^{17}O$ and $\Delta^{17}O$) as well as corresponding concentrations in TSP samples during "Earth Summit Mission" scientific expedition in spring 2022. The gray shaded area denotes local nighttime.

Table 1. The measured nitrite (and nitrate) concentration and isotopic signatures in surface soil collected in the Rongbuk Valley.

Soil sample ID	NO_2^-				NO_3^-			
	Conc.(ng g^{-1})	$\delta^{15}N$	$\delta^{18}O$	$\Delta^{17}O$	Conc.(ng g^{-1})	$\delta^{15}N$	$\delta^{18}O$	$\Delta^{17}O$
East-1	67.7	-12.0	6.1	3.3	1127.3	-2.7	23.4	5.7
East-2	76.1	-11.9	2.7	2.2	1098.3	1.3	18.1	3.8
East-3	82.3	-14.6	6.0	3.3	2978.1	-0.3	25.4	6.6
West-1	88.6	-10.1	8.9	1.6	3176.5	-3.1	44.5	13.4
West-2	106.2	-7.0	11.4	1.5	2880.3	-1.2	22.1	6.2
West-3	179.3	-5.2	12.7	1.4	7686.9	-3.4	35.8	11.4
South-1	53.8	-13.2	12.7	6.7	3651.2	-0.6	32.6	10.1
South-2	42.3	-9.0	18.1	7.3	1683.2	-2.2	49.3	14.8
South-3	48.9	-10.3	12.4	6.7	385.5	-2.4	45.7	14.9

370

3.3 Surface soil nitrite concentration and isotopic signature

The concentration of soil NO_2^- (and NO_3^-) as well as the corresponding isotopic signatures are displayed in Table 1. The soil NO_2^- content on the west slope of Rongbuk Valley (on average 124.7 ng g^{-1}) is higher than that observed on the east and south sides (75.3 ng g^{-1} and 48.3 ng g^{-1}, respectively). ~~High soil NO_2^- and NO_3^- concentrations were observed on the west and east slopes of the Rongbuk valley relative to that on the south side of the sampling site.~~ The mean surface soil

377 NO_2^- and NO_3^- in the Rongbuk Valley were 82.8 and 2740.8 ng g^{-1}, respectively. The soil NO_3^-

378 concentrations are significantly higher than the NO_2^- by a factor of 8 ~ 40. In general, the measured

379 soil NO_3^- concentrations at the Rongbuk valley are significantly lower than other remote regions of

380 TP (i.e., 23.1 μg g^{-1} at Naqu, 8.4μg g^{-1} at ~~Bangda~~Yangbajing), while soil NO_2^-concentrations are

381 comparable to these reports (i.e., 90.3 ng g^{-1} at Naqu,131.2 ng g^{-1} at Yangbajing) (Wang et al., 2019).

382 Soil $\delta^{15}N(NO_2^-)$ values ranged from -13.2‰ to -5.2‰ (on average -10.4‰), which are comparable

383 to TSP $\delta^{15}N(NO_2^-)$ (-7.3‰). In comparison, we observed positive soil $\delta^{18}O(NO_2^-)$ and $\Delta^{17}O(NO_2^-)$,

384 ranging from 2.7‰ to 18.1‰ (on average 10.5‰) and 1.4‰ to 7.3‰ (on average 3.8‰),

385 respectively, in contrast to the negative $\delta^{18}O(NO_2^-)$ and near-zero $\Delta^{17}O(NO_2^-)$ observed in TSP

386 samples. The determined soil $\delta^{18}O(NO_2^-)$ is comparable to that in laboratory incubated soil (11.8‰

387 ~ 12.5‰) (Lewicka-Szczebak et al., 2021).

4 Discussion

389   The significant contrast in NO_2^- concentrations between TSP and $PM_{2.5}$ samples, as shown in

390 Figure 1, suggests that at the sampling site atmospheric particle NO_2^- overwhelmingly exists in

391 coarse particles. This observation is consistent with previous studies across the TP, which also

392 reported the absence of NO_2^- in fine mode particles ($PM_{2.5}$ and $PM_{1.0}$) using either online real-time

393 instrument or offline filter sampling (Decesari et al., 2010; Xu et al., 2020; Xu et al., 2023; Zhao et

394 al., 2020), while relatively high levels of TSP NO_2^- have been reported (Bhattarai et al., 2019;

395 Bhattarai et al., 2023; Tripathee et al., 2017). In general, the chemical sources of particle NO_2^- in

396 the atmosphere encompass the uptake of HONO, particulate nitrate photolysis, and the NO_2-related

397 reactions (i.e., photo-enhanced uptake of NO_2 on mineral dust, heterogeneous reaction of NO_2 on

398 the surface of aerosol) (Nie et al., 2012; Vandenboer et al., 2014a; Chen et al., 2019; Shang et al.,

399 2021), as summarized in Table 2. In addition to these in-situ atmospheric processes, growing

400 evidence has revealed that long-range transport of atmospheric pollutants from South Asia also

401 contributes considerably to aerosol loadings in TP in the spring (Kang et al., 2019; Bhattarai et al.,

402 2023; Zhao et al., 2020), which may also bring nitrite along with other pollutants. Moreover, the

403 lifting of surface dust can also contribute to the atmospheric coarse particles and significantly

404 influence the chemical composition of TSP (Zhang et al., 2021a; Pokharel et al., 2019), and therefore

405 soil nitrite could also be a potential source for TSP NO_2^-. In the following discussion, we examine

406 the potential importance of the abovementioned processes to the observed high NO_2^- content in

407 coarse particle and discern the most likely ones.

408 **Table 2.** Particulate nitrite concentration and formation pathways/sources compiled in the literature.
409

Site	Period	NO_2^- Conc. (mean, ng m^{-3})	Formation pathways/Sources	Reference
QOMS station	April 2017	60	Biomass burning emission transported from South Asia	Bhattarai et al., 2023
Bakersfield, California	May–July 2010	150	HONO uptake on lofted alkaline soil particles.	VandenBoer et al., 2014
Jinan, China	November 2013 − January 2014	2080	Heterogeneous reactions of NO_2	Wang et al., 2015
Seoul, Korea	May−July, 2005	1410	Heterogeneous reactions of NO_2	Song et al., 2009
Shanghai, China	June 2020	210	Heterogeneous reactions of NO_2, reduction of NO_2 by S(IV)	Shang et al., 2021
Mt.Heng, China	April 2009	2500	Surface TiO_2 photocatalysis of NO_2	Nie et al., 2012

410 **4.1 The potential effects of atmospheric chemistry on NO_2^- in TSP**

411 Increasing evidence supports particulate nitrate photolysis as an important source of

412 atmospheric HONO especially in pristine atmosphere, with NO_2^- serving as the intermediate in the

413 subsequent gas-particle partition process (Andersen et al., 2023; Ye et al., 2016). In theory,

414 particulate NO_2^- (and HONO) produced from particulate nitrate photolysis might be associated with

415 extremely negative $\delta^{15}N$ values, due to the significant nitrogen isotopic fractionation effect during

416 nitrate photolysis (Erbland et al., 2013). For example, NO_2^- in water of hypersaline ponds and soil

417 of McMurdo Dry Valleys, Antarctica, produced from the NO_3^- photolysis, were characterized by

418 significantly negative $\delta^{15}N$ values (< -80‰) (Peters et al., 2014). However, $\delta^{15}N(NO_2^-)$ in this study

419 was only ~2‰ lower than the $\delta^{15}N(NO_3^-)$ in TSP samples collected during this campaign (on

420 average (-5.3 ± 3.3)‰, Text S1) and that at the QOMS stations (annual average of (-5.1 ± 2.3) ‰)

421 (Wang et al., 2020). The similarity in $\delta^{15}N$ isotopes between NO_2^- and NO_3^- suggests particulate

422 nitrate photolysis is unlikely to be the primary source of the TSP NO_2^-.

423 In addition to nitrate photolysis, the absorption of HONO on alkaline aerosols (i.e., lofted dust

424 and road salt particles) can also result in accumulation of NO_2^- into the particle phase (Vandenboer

425 et al., 2014a; Chen et al., 2019). For example, *VandenBoer et al.* observed a synchronous

426 enhancement of fine particle NO_2^- (as high as 730 ng m^{-3}) alongside the buildup of HONO (up to

1.37 ppbv) after sunset in an agricultural site (Vandenboer et al., 2014a). However, the levels of HONO in terrestrial background environments, typically on the order of dozens of pptv (Ye et al., 2023), are obviously too low to support the observed unexpectedly high levels of particulate NO_2^- (up to 1300 ng m^{-3}). What is more, previous studies indicted the HONO uptake predominately occurs on fine particles (Wang et al., 2015; Chen et al., 2019; Shang et al., 2021), while our observations indicated NO_2^- only exists in coarse particles.

The uptake of NO_2 on mineral dust has also been identified as a significant route for the formation of particulate NO_2^- or gas-phase HONO (Nie et al., 2012; Ndour et al., 2008). For example, *Nie et al.* found a significantly enhanced NO_2^- in coarse particle during daytime in a dust storm event in Mt. Heng (up to 4.5 μg m^{-3}) (Nie et al., 2012). The proposed mechanism is initiated ~~initialed~~ by photo-enhanced conversion~~photocatalysis~~ of NO_2 to NO_2^- via photo-produced electrons on surface of dust. Nevertheless, given the relatively small NO_2 uptake coefficients (generally lower than 10^{-6} on mineral dust or salt surface) (Yu et al., 2021; Bao et al., 2022; Xuan et al., 2025) and the low concentration of NO_2 in pristine environment of TP (e.g., ~ 140 pptv at Namco (Wang et al., 2023), and would be even lower at Mt. Qomolangma), such high levels of particulate NO_2^- are beyond the capacity of NO_2 heterogeneous reactions.

Other than the above-mentioned rationales, the atmospheric physicochemical processes leading to NO_2^- production would influence both fine and coarse-mode particles, and some of the processes (e.g., HONO uptake) preferentially interact with fine-mode particles. However, the observation indicated NO_2^- only exists in TSP but not PM$_{2.5}$, suggesting atmospheric physicochemical processes are unlikely to account for the elevated levels of NO_2^- in TSP.

4.2 Potential effect of ~~biomass burning emissions~~atmospheric pollutants in South Asia via long-range transport

There is a growing body of compelling evidence indicating that the elevated aerosol loadings and chemical species in TP during spring, i.e., black carbon (Cong et al., 2015; Kang et al., 2019) and soluble components (Dasari et al., 2023; Bhattarai et al., 2023; Lin et al., 2021; Wang et al., 2020; Zhao et al., 2020) are significantly linked to biomass burning emissions from South Asia, which can penetrate into TP via long range transport. Recently, *Bhattarai et al.* observed

455 synchronously elevated water-soluble nitrogen compounds (i.e., NO_2^-, NH_4^+, NO_3^-), levoglucosan

456 (a molecule marker for biomass burning) and bulk $\delta^{15}N$ signatures in TSP at QOMS station, once

457 upon the arrival of biomass burning plumes from South Asia (Bhattarai et al., 2023). Specially, they

458 found that TSP NO_2^- averaged 60 ng m^{-3} during the spring biomass burning influenced episodes,

459 while NO_2^- was always below the detection limit in other seasons (Bhattarai et al., 2023). This

460 suggests that biomass burning events in South Asia and the subsequent long-range transport could

461 contribute to accumulation of NO_2^- in aerosols in Tibet.

462 In this study, the mass concentrations and compositions of water-soluble ions, including SO_4^{2-},

463 NO_3^-, NH_4^+ and TSP NO_2^-, also varied substantially throughout the springtime campaign (Fig.1).

464 The potential effect of South Asian pollutants on our observations was explored by analyzing the

465 air masses origins during the sampling period. To evaluate the potential effects of South Asian

466 pollutants on our observations, we further analyzed the air masses origins during the sampling

467 campaign. As shown in Figure 35, during the first-half of the campaign (, i.e., before May 1stApril

468 30th), air masses mainly predominately originated from or passed through northern India and Nepal

469 with intensive human activities and numerous fire hotspots (represented by the dense red dots in

470 Figure 5), indicating the potential impact of South Asia pollutants on aerosol loadings of TP.

471 Correspondingly, elevated concentrations of secondary inorganic ions (i.e., NH_4^+, NO_3^- and SO_4^{2-})

472 in TSP and PM$_{2.5}$ were observed before April 30th, which are comparable to the values of previous

473 reports in QOMS station when arrived air masses experiencing severe biomass burning

474 emissions(Bhattarai et al., 2023; Lin et al., 2021). Meanwhile, elevated levels of TSP NO_2^- (625 ±

475 457 ng m^{-3}) was observed during this biomass burning-impacted period, and $\delta^{15}N(NO_2^-)$ values

476 exhibited substantial variability. TSP samples collected during daytime of April 27th and night of

477 April 28th are associated with high NO_2^- concentrations and $\delta^{15}N(NO_2^-)$ values. In comparison, TSP

478 NO_2^- in other samples were significantly ^{15}N-depleted. Assuming that biomass burning emission

479 accounted for the two high $\delta^{15}N(NO_2^-)$ samples (Bhattarai et al., 2023), the observed relatively low

480 $\delta^{15}N(NO_2^-)$ in other samples before April 30th likely indicated the potential contribution from

481 additional emission sources.

482 From May 1st to May 6th, air masses originated primarily from the inside of the TP or

483 surroundings and none of the fire hotspot was detected at the whole TP and along the air mass

19

484 trajectories (Figure 5), potentially excluding the influence of biomass burning and anthropogenic

485 emissions during this period. Accompanied by this significant shift in air mass origins, the

486 concentrations of NH_4^+, NO_3^- and SO_4^{2-} in both $PM_{2.5}$ and TSP, as well as the TSP NO_2^- apparently

487 decreased. In particular, NH_4^+ in most $PM_{2.5}$ and TSP samples were below the detection limit during

488 this period. Furthermore, K^+ in $PM_{2.5}$, a common tracer for biomass burning, declined from 269 ±

489 432 ng m^{-3} before April 30th to 22 ± 12 ng m^{-3} after April 30th, with the difference being statistically

490 significant ($p < 0.05$). Meanwhile, the average TSP NO_2^- also declined significantly from 625 ± 457

491 ng m^{-3} before April 30th to 147 ± 145 ng m^{-3} after April 30th. Note substantially high levels of TSP

492 NO_2^- were also observed on several days after April 30th, i.e., during daytime of May 3rd (~ 400 ng

493 m^{-3}). Although the TSP NO_2^- concentrations varied in wide range after April 30th, the $\delta^{15}N(NO_2^-)$

494 was relatively stable and comparable to that determined before April 30th (except for the two high

495 $\delta^{15}N(NO_2^-)$ samples). while from May 1st to May 6th the air masses originated from the inside of the

496 TP with rare open fires. Accompanied by this shift in air mass origins, the concentrations of NH_4^+,

497 NO_3^- and SO_4^{2-} in both $PM_{2.5}$ and TSP, as well as the TSP NO_2^- apparently decreased, suggesting

498 that these species in $PM_{2.5}$ and TSP should be controlled or closely related to biomass burning events

499 in South Asia and the subsequent long-range transport of biomass burning pollutants.

500   In short summary, these results likely suggest the significant impact of South Asia pollutants

501 (i.e., biomass burning emissions) through long-range transport on the TSP NO_2^-, especially for

502 samples collected before April 30th. However, it is difficult for the long-range transport to explain

503 why NO_2^- is predominately present in coarse particles, as fine mode particle is typically easier to be

504 transported in principle. While further studies need to be conducted to find out the exact reasons,

505 one possibility is that the size partition of fine particle NO_2^- toward the coarse mode range during

506 transport. Similar size shifts of NO_3^- have been observed and used to explain the enrichment of NO_3^-

507 in coarse-mode aerosols in marine environment (Matsumoto et al., 2009). In addition, the coarse

508 mode particles in this study contain more alkaline species (Figure 2), which makes nitrite more

509 stable in TSP during the transport or more stably exist in TSP after being uptake when the polluted

510 air masses reaching TP. For the period after April 30th, since air masses originated from clean regions

511 with little to no biomass burning sources, other sources of nitrite might be required.

512   However, although biomass burning activities indeed emit various nitrogen compounds into

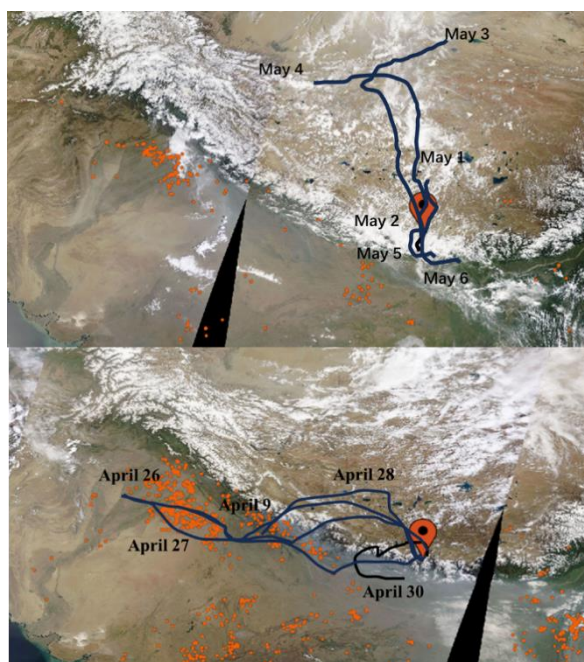**Figure 35.** The modelled six-day air-mass back trajectories during "Earth Summit Mission" scientific expedition in spring 2022 (a: from May 1st to May 6th; b: April 26th to April 30th). The active fire spots captured by MODIS (https://worldview.earthdata.nasa.gov, the red dots in the figure) are also presented.

4.3 The potential effects of lofted dust

Previous reports have confirmed that wind-blown mineral dust contributed significantly to coarse mode aerosols in TP (Kang et al., 2016; Zhang et al., 2021a). Notably, surface soil collected from the Rongbuk valley is characterized with elevated NO$_2^-$ concentration (up to 180 ng g^{-1}, Table 1). The surface soil NO$_2^-$ is expected to mainly reside in the coarse mode after suspended in the atmosphere (Drakaki et al., 2022), consistent with our observations that particle NO$_2^-$ was predominately confined into coarse particle. The unique environment of Rongbuk valley, characterized by exposed surface soil and strong wind (reaching as high as 9 m/s during this

campaign) could facilitate the resuspension of soil components into the atmosphere. Furthermore, small localized tornadoes were frequently observed before May 1st, while the snow events occurred in April 30th would reduce the soil-derived dust emission by increasing the snow coverage and enriching the soil moisture. In fact, concentrations of Ca^{2+} in TSP, which predominately originate from dust emission, also declined to some extent after May 1st.

In addition, the similarity in $\delta^{15}N$ of NO_2^- between TSP (-7.3 ± 3.1‰) and the surface soil (-7.3 ± 3.1‰ vs. -10.3 ± 3.0‰) also likely supports that locally emitted surface soil may contribute to the observed high levels of TSP NO_2^-. But one should note that the oxygen isotopes ($\delta^{18}O$ and $\Delta^{17}O$) of TSP NO_2^- were significantly lower compared to and that in soil NO_2^- are different, indicating that the original soil NO_2^- oxygen isotope may have been modified after resuspension. This discrepancy could be explained by the potential oxygen isotope exchanges between TSP NO_2^- and aerosol liquid water (fractionation effect of $^{18}\varepsilon_{eq} \approx 16‰$ at local temperature, T = 270K, $^{18}\varepsilon_{eq} = -0.12$ T + 48.79 (Buchwald and Casciotti, 2013)), which will tend to deplete both the initial $\delta^{18}O(NO_2^-)$ and $\Delta^{17}O(NO_2^-)$.

We noted the oxygen isotope exchange process between NO_2^- and H_2O also occurs in surface soil. Previous study indicated that in high-altitude arid regions of TP (i.e., >5000m), denitrification process dominated the surface soil NO_2^- production, accounting for ~75% (Wang et al., 2019). Soil NO_2^- generated from denitrification process is expect to inherit the $\Delta^{17}O$ signatures of substrate NO_3^-. In this study, the surface soil $\Delta^{17}O(NO_3^-)$ were positive with average values of 9.6‰ (Table 1). The positive soil $\Delta^{17}O(NO_3^-)$ have been observed on arid environments (Wang et al., 2016), such as desert soil, where the low water moisture favors the preservation of atmospherically derived NO_3^-. One could estimate that soil $\Delta^{17}O(NO_2^-)$ derived from the denitrification would be 9.6‰, nitrite from other sources (e.g., nitrification) should possess zero $\Delta^{17}O$, thus in total nitrite in soil should possess $\Delta^{17}O$ of ~7.2‰ (estimated as $0.75 \times \Delta^{17}O(NO_3^-)$). However, the determined soil $\Delta^{17}O(NO_2^-)$ (3.8‰) is significantly lower compared to the estimated soil $\Delta^{17}O(NO_2^-)$, indicating the occurrence of exchange process between soil water and NO_2^-, which would reduce the soil $\Delta^{17}O(NO_2^-)$ to some extent. The exchange process between soil water and NO_2^- is particularly evident in west slope of Rongbuk Valley, where soil $\Delta^{17}O(NO_2^-)$ is as low as 1.5‰ while soil $\Delta^{17}O(NO_3^-)$ is on average 10.3‰. Soil $\Delta^{17}O(NO_2^-)$ should be erased to near-zero if exchange process between soil water and

NO$_2^-$ was efficient. Therefore, the fact that the observed soil Δ^{17}O(NO$_2^-$) remain above 0‰ indicates unfavorable conditions for the oxygen isotope exchange process, likely due to the extremely low soil moisture content (~1%) in surface soil (Ma et al., 2023).

~~soil δ^{18}O(NO$_2^-$) once~~ Upon ~~resuspended~~ resuspension into atmosphere, the soil-derived dust aerosols usually exhibited a certain degree of hygroscopicity (Tang et al., 2016; Chen et al., 2020), allowing the absorption of water molecule on dust aerosol. For example, the aerosol water was determined to account for ~20% of the total PM$_{10}$ mass during Saharan dust plumes (Cardoso et al., 2018). Based on laboratory experiment, Tang et al., 2019 reported that Asian dust also exhibited substantial hygroscopic property and revealed that the water-soluble inorganic ions, such as Cl$^-$, SO$_4^{2-}$ and NO$_3^-$ played a critical role in the absorption of water molecules on dust aerosol (Tang et al., 2019). In the present study, the SO$_4^{2-}$ and NO$_3^-$ account for ~30% of the total mass of water-soluble ions in TSP, implying the potential uptake of water vapor on aerosol surface. In addition to water-soluble ions, the hygroscopicity of mineral dust also depend on the surface areas, and wind-blown dust experiences a substantial increase in surface area after being lifted into the atmosphere, enhancing its capacity for water uptake (Chen et al., 2020; Seisel et al., 2004). The hygroscopicity of dust aerosol is expected to accelerate the oxygen isotope exchanges between NO$_2^-$ and aerosol liquid water.~~ ~~ The atmospheric water vapor δ^{18}O isotope in TP is determined to be significantly negative (approximately -35‰ to -15‰ at a remote site in TP with altitude of ~ 4200m) (Yu et al., 2015). Similarly, t~~T~~he oxygen isotope exchange between NO$_2^-$ and H$_2$O would also homogenize and erase original soil Δ^{17}O(NO$_2^-$) signals, because aerosol liquid water is ~~content is at least three orders of magnitude higher than NO$_2^-$ (Text S2) and~~ characterized by negligible Δ^{17}O values (Luz and Barkan, 2005). Consequently, isotope exchange with aerosol water would further reduce both δ^{18}O and Δ^{17}O of TSP NO$_2^-$, effectively masking the original isotopic signature inherited from surface soil.

We also noted that NO$_2^-$ in surface soil is significantly lower than NO$_3^-$, by ~~up to 40~~on average 35 times (Table 1), contrasting with the chemical compositions in TSP. ~~Soil samples were sieved to less than 60 mesh (~250 μm), to be in similar order with the diameters of TSP. We speculate that the size distribution of NO$_2^-$ in surface soil maybe different with NO$_3^-$ if resuspended surface soil was the primary source of TSP.~~ It is important to note that during the complex dust generation and

aerosolization processes, water-soluble ions exhibit significant chemical enrichment relative to that in parent soil (Wu et al., 2022; Gao et al., 2023). For example, Wu et al., 2022 reported that contents of nitrate in sand dust-derived PM_{10} is higher than the original soil samples by 2~80 times, while sulphate can be up to 500 times higher than the original soil. Although the enrichment of nitrite has not been evaluated to the extent of our knowledge, we propose that the observed discrepancy of nitrate/nitrite ratio between TSP and surface soil can be reconciled if the nitrite is enriched more efficiently than nitrate during dust aerosolization, i.e., by a factor of 30.

To further assess the potential contribution of resuspended soil to elevated nitrite in TSP, we conducted a rough estimation based on laboratory investigations from Wu et al. (2022). First, the springtime TSP concentrations observed in the nearby QOMS station is used (65.1 ± 50.9 μg m^{-3}; (Liu et al., 2017)), as TSP mass concentrations surrounding the Base camp were not available. Second, we assumed the nitrite content in soil-derived coarse particles to be similar to that of nitrate (0.2%) in laboratory-generated dust aerosol from natural sandy and gravel soils (Wu et al., 2022), which is comparable to the soil texture of the Rongbuk Valley. This assumption can also explain the comparable amounts of nitrite and nitrate observed in TSP samples in this study. Results shown that the concentrations of nitrite in TSP can be approximately 130 ± 102 ng m^{-3}, on the same order with the observed nitrite concentration in TSP after April 30th (147 ± 145 ng m^{-3}) but substantially lower than that before April 30th (625 ± 457 ng m^{-3}). Therefore, we speculate that the resuspension of surface soil may account for the observed TSP nitrite after April 30th, whereas the biomass burning and soil together co-contributed to the high TSP nitrite before April 30th. This is also consistent with the shift of air mass origins, which clearly indicated that airmasses before April 30th is significantly impacted by the biomass burning emissions, and after April 30th airmasses primarily originated from clean regions. While we acknowledge that this simplistic estimation is subject to substantial uncertainty, it provides a first-order assessment supporting the hypothesis that wind-blown soil dust contributes to coarse-mode particulate nitrite. Previously, wind-blown mineral dust has been verified as a potential source for aerosol water-soluble ions (Engelbrecht et al., 2016; Wu et al., 2022; Wu et al., 2012) and dust aerosol is also recognized as one of the important aerosol types over TP (Pokharel et al., 2019).

5 Conclusion and Implications

619 Unexpectedly high levels of ~~NO₂⁻ associated with~~ coarse-particle ~~NO₂⁻~~ were observed in the

620 pristine environment at Mt. Qomolangma in the spring, 2022. After examining the potential

621 contributions of various NO_2^- sources with assistance from air mass back-trajectory and isotope

622 analyses, we suggest that both soil-derived nitrite and long-range transport of pollutants from South

623 Asia may contribute to coarse-particle NO_2^- during spring at Mt. Qomolangma. This is also

624 consistent with previous reports showing that dust and biomass burning emission through long-

625 range transport from South Asia are the predominant contributors to the springtime aerosol loadings

626 over TP (Zhao et al., 2020; Pokharel et al., 2019). The nitrite concentrations and isotopes further

627 indicated that soil-derived nitrite likely serves as a baseline source of atmospheric NO_2^-, maintaining

628 the background levels of TSP NO_2^- at this pristine site, reflected by the relatively stable isotopes

629 when soil-derived nitrite predominated. ~~Moreover~~In addition, air masses originating from South

630 Asia would result in elevated levels of NO_2^- observed before April 30th by bringing additional

631 biomass burning and anthropogenic pollutants,~~also contribute to elevated NO₂⁻ by bringing biomass~~

632 ~~burning pollutants~~, as evidenced by the ~~observed higher TSP NO₂⁻~~more varied isotopes before ~~May~~

633 ~~1st~~April 30th compared to after that day when air mass origins shifted from South Asia to Central

634 and North Tibet. However, the detailed mechanisms of nitrite enriched on the coarse particle remain

635 unknown and need further explorations. ~~The dual-contribution of soil nitrite and long-range~~

636 ~~transport of pollutants from South Asia to the observed TSP NO₂⁻ at Mt. Qomolangma is also~~

637 ~~consistent with the dynamics of NO₂⁻ isotopic signatures, as the isotopes were more varied during~~

638 ~~the first half of the campaign when both soil and long-range transport-related nitrite contributed,~~

639 ~~while in the second half of the campaign the isotopes were more stable when soil nitrite~~

640 ~~predominated. The effect of long-range transport from South Asia, however, would be likely mainly~~

641 ~~through the transport of nitrite precursors (e.g., NO₂, HONO) rather than nitrite itself as there is~~

642 ~~likely no nitrite in biomass burning plumes (Lindaas et al., 2021; Juncosa Calahorrano et al., 2021;~~

643 ~~Li et al., 2003). Nevertheless, it is currently unknown why such precursors would selectively interact~~

644 ~~with coarse mode particles, resulting in nitrite predominately resides in coarse-mode particles.~~

645 ~~Further investigation should be conducted to clarify the reason.~~

646 In the atmosphere, photolysis of particle nitrite can produce OH radical and NO, the latter is

647 essential for the formation of atmospheric oxidants and secondary aerosols. ~~Our results highlight~~

648 ~~that soil nitrite could also be directly lofted into atmosphere and potentially acting as an important~~
649 ~~NO$_x$ and HONO source, a previously unrecognized soil atmosphere interactions which may greatly~~
650 ~~impact the atmospheric environment (Figure 4).~~ Moreover, the~~The~~ elevated levels of particle NO$_2^-$
651 may serve as an important HONO source through the gas-to-particle partition process (Vandenboer
652 et al., 2014a), and the thermodynamic equilibrium between particulate nitrite and HONO
653 ([pN(III)]/[HONO] ratio) is primarily governed by the particle acidity and liquid water content
654 (LWC) in theory (Fountoukis and Nenes, 2007; Vandenboer et al., 2014a; Chen et al., 2019). Based
655 on the observed TSP NO$_2^-$ and estimated ratio of [pN(III)]/[HONO] (from 4.8 to 10.6, Text S2), we
656 can estimate the potential level of atmospheric HONO if the partition ever occurs at this site
657 (Vandenboer et al., 2014b), and result indicates HOHO would be at 8 ~ 15 pptv, on the same order
658 with the observations at a central Tibetan site (~ 30 pptv at Namco (Wang et al., 2023)). ~~Therefore,~~
659 ~~we suspect that the elevated levels of particle NO$_2^-$ by lofted soil may significantly impact local~~
660 ~~reactive nitrogen cycling and atmospheric oxidation capacity by acting as source of reactive nitrogen~~
661 ~~species through photolysis or thermodynamic partitioning processes in the pristine environment of~~
662 ~~TP (Li, 1994; Song et al., 2009; Wang et al., 2015; Chen et al., 2019).~~ Given that TSP concentrations
663 usually reach maximum during spring over TP, i.e., 65 ± 51 µg m^{-3} at the nearby QOMS station (Liu
664 et al., 2017), our findings suggest that the coarse-particle may serve as a potential source of
665 atmospheric HONO and NO$_x$ assuming the TSP are associated with nitrite. Although the coarse-
666 particle tend to deposit rapidly within hours, their potential to influence local atmospheric chemistry
667 remains important to some extent, particularly considering the frequent dust events in TP (loose
668 arid/semiarid surface, sparse vegetation, and strong winds.(Long et al., 2025)) and the ubiquity of
669 long-range transport of biomass burning emissions from South Asia during this season. The impact
670 of the TSP nitrite on the budget of NOx, HONO and OH radicals especially in the background
671 atmosphere could be investigated using regional or global atmospheric transport model, once the
672 detailed mechanism regarding the sources and chemistry of TSP nitrite been elucidated. In summary,
673 our results highlight the need for further investigation into the sources, partitioning, and chemical
674 reactivity of aerosol-phase nitrite, particularly in the pristine Tibetan Plateau, where even small
675 inputs of NO$_x$ or HONO can disproportionately affect oxidant budgets and reactive nitrogen cycling
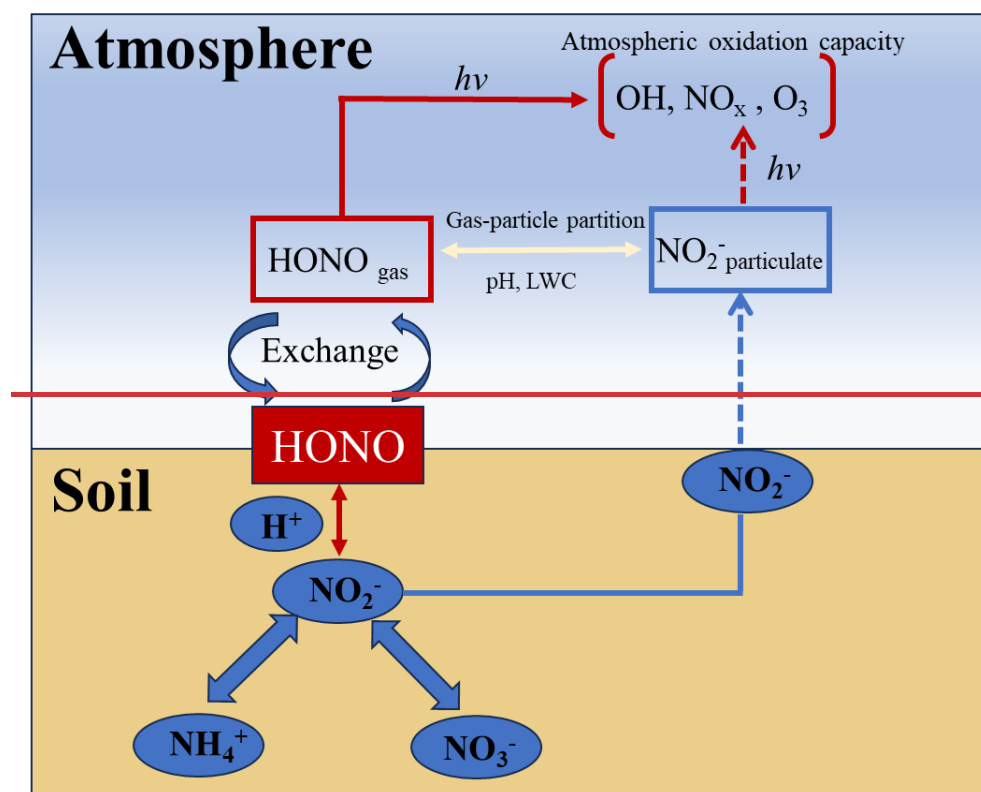
676

677

Figure 4 ~~The conceptual model illustrating the impact of soil nitrite on the atmospheric reactive nitrogen cycling and atmospheric oxidation capacity. Through bi-direction exchange, soil nitrite is an important source of atmospheric HONO. Moreover, the wind-blown soil nitrite can also contribute to atmospheric HONO and NO$_x$ through thermodynamic partition process or photolysis.~~

Conflicts of interest

The authors declare that they have no conflicts of interest.

Autor contribution:

L.G designed the research, interpreted the data; L.G and Z.Z prepared the manuscript with contributions from all co-authors; Z.Z., Y.W., C.Y., T.Z., C.Z., Z.J., and P.C., conducted the field sampling and laboratory measurements; L.G, Z.Z., and P.C., acquired funding; L.G., S.K., and C.Y. reviewed and edited the manuscript. All authors have given approval to the final version of the manuscript.

Data availability

The data supporting the findings of this study are available in the archival repository at: https://doi.org/10.6084/m9.figshare.28188320.v1

References

Albertin, S., Savarino, J., Bekki, S., Barbero, A., and Caillon, N.: Measurement report: Nitrogen isotopes (δ^{15}N) and first quantification of oxygen isotope anomalies (Δ^{17}O, δ^{18}O) in atmospheric nitrogen dioxide, Atmos. Chem. Phys., 21, 10477-10497, 10.5194/acp-21-10477-2021, 2021.

Andersen, S. T., Carpenter, L. J., Reed, C., Lee, J. D., Chance, R., Sherwen, T., Vaughan, A. R., Stewart, J., Edwards, P. M., and Bloss, W. J. J. S. A.: Extensive field evidence for the release of HONO from the photolysis of nitrate aerosols, Science Advances, 9, eadd6266, 2023.

Bao, F., Cheng, Y., Kuhn, U., Li, G., Wang, W., Kratz, A. M., Weber, J., Weber, B., Pöschl, U., and Su, H.: Key Role of Equilibrium HONO Concentration over Soil in Quantifying Soil–Atmosphere HONO Fluxes, Environmental Science & Technology, 56, 2204-2212, 10.1021/acs.est.1c06716, 2022.

Bhattarai, H., Wu, G., Zheng, X., Zhu, H., Gao, S., Zhang, Y.-L., Widory, D., Ram, K., Chen, X., and Wan, X.: Wildfire-Derived Nitrogen Aerosols Threaten the Fragile Ecosystem in Himalayas and Tibetan Plateau, Environmental Science Technology, 2023.

Bhattarai, H., Zhang, Y.-L., Pavuluri, C. M., Wan, X., Wu, G., Li, P., Cao, F., Zhang, W., Wang, Y., and Kang, S.: Nitrogen speciation and isotopic composition of aerosols collected at Himalayan forest (3326 m asl): seasonality, sources, and implications, Environmental Science Technology, 53, 12247-12256, 2019.

Buchwald, C. and Casciotti, K. L.: Isotopic ratios of nitrite as tracers of the sources and age of oceanic nitrite, Nature Geoscience, 6, 308-313, 10.1038/ngeo1745, 2013.

Casciotti, K. L., Böhlke, J. K., McIlvin, M. R., Mroczkowski, S. J., and Hannon, J. E.: Oxygen isotopes in nitrite: Analysis, calibration, and equilibration, Analytical Chemistry, 79, 2427-2436, 2007.

Chen, Q., Edebeli, J., McNamara, S. M., Kulju, K. D., May, N. W., Bertman, S. B., Thanekar, S., Fuentes, J. D., and Pratt, K. A.: HONO, Particulate Nitrite, and Snow Nitrite at a Midlatitude Urban Site during Wintertime, ACS Earth and Space Chemistry, 3, 811-822, 10.1021/acsearthspacechem.9b00023, 2019.

Cong, Z., Kang, S., Kawamura, K., Liu, B., Wan, X., Wang, Z., Gao, S., and Fu, P.: Carbonaceous

aerosols on the south edge of the Tibetan Plateau: concentrations, seasonality and sources, Atmos. Chem. Phys., 15, 1573-1584, 10.5194/acp-15-1573-2015, 2015.

Dasari, S., Paris, G., Pei, Q., Cong, Z., and Widory, D.: Tracing the origin of elevated springtime atmospheric sulfate on the southern Himalayan-Tibetan plateau, Environmental Science: Advances, 2, 1110-1118, 2023.

Decesari, S., Facchini, M., Carbone, C., Giulianelli, L., Rinaldi, M., Finessi, E., Fuzzi, S., Marinoni, A., Cristofanelli, P., and Duchi, R. J. A. C.: Chemical composition of PM10 and PM1 at the high-altitude Himalayan station Nepal Climate Observatory-Pyramid (NCO-P)(5079 m asl), Atmospheric Chemistry Physics, 10, 4583-4596, 2010.

Drakaki, E., Amiridis, V., Tsekeri, A., Gkikas, A., Proestakis, E., Mallios, S., Solomos, S., Spyrou, C., Marinou, E., Ryder, C. L., Bouris, D., and Katsafados, P.: Modeling coarse and giant desert dust particles, Atmos. Chem. Phys., 22, 12727-12748, 10.5194/acp-22-12727-2022, 2022.

Erbland, J., Vicars, W. C., Savarino, J., Morin, S., Frey, M. M., Frosini, D., Vince, E., and Martins, J. M. F.: Air–snow transfer of nitrate on the East Antarctic Plateau Part 1: Isotopic evidence for a photolytically driven dynamic equilibrium in summer, Atmospheric Chemistry and Physics, 13, 6403-6419, 10.5194/acp-13-6403-2013, 2013.

Fang, Y., Koba, K., Wang, X., Wen, D., Li, J., Takebayashi, Y., Liu, X., and Yoh, M.: Anthropogenic imprints on nitrogen and oxygen isotopic composition of precipitation nitrate in a nitrogen-polluted city in southern China, Atmos. Chem. Phys., 11, 1313-1325, 2011.

Felix, J. D. and Elliott, E. M.: Isotopic composition of passively collected nitrogen dioxide emissions: Vehicle, soil and livestock source signatures, Atmospheric Environment, 92, 359-366, 10.1016/j.atmosenv.2014.04.005, 2014.

Fountoukis, C. and Nenes, A.: ISORROPIA II: a computationally efficient thermodynamic equilibrium model for K^+–Ca^{2+}–Mg^{2+}–NH_4^+–Na^+–SO_4^{2-}–NO_3^-–Cl^-–H_2O aerosols, Atmospheric Chemistry and Physics, 7, 4639-4659, 2007.

Geng, L., Alexander, B., Cole-Dai, J., Steig, E. J., Savarino, J., Sofen, E. D., and Schauer, A. J.: Nitrogen isotopes in ice core nitrate linked to anthropogenic atmospheric acidity change, Proceedings of the National Academy of Sciences, 111, 5808-5812, 2014.

Hastings, M. G., Sigman, D. M., and Lipschultz, F.: Isotopic evidence for source changes of nitrate in rain at Bermuda, Journal of Geophysical Research: Atmospheres, 108, 10.1029/2003jd003789, 2003.

Homyak, P. M., Vasquez, K. T., Sickman, J. O., Parker, D. R., and Schimel, J. P.: Improving nitrite analysis in soils: Drawbacks of the conventional 2M KCl extraction, Soil Science Society of America Journal, 79, 1237-1242, 2015.

Hsu, S. C., Liu, S. C., Huang, Y. T., Chou, C. C., Lung, S. C., Liu, T. H., Tu, J. Y., and Tsai, F.: Long-range southeastward transport of Asian biosmoke pollution: Signature detected by aerosol potassium in northern Taiwan, Journal of Geophysical Research: Atmospheres, 114, 2009.

Immerzeel, W. W., Van Beek, L. P., and Bierkens, M. F.: Climate change will affect the Asian water towers, Science, 328, 1382-1385, 2010.

Jacobi, H.-W., Kleffmann, J. r., Villena, G., Wiesen, P., King, M., France, J., Anastasio, C., and Staebler, R.: Role of nitrite in the photochemical formation of radicals in the snow, Environmental science technology, 48, 165-172, 2014.

Juncosa Calahorrano, J. F., Lindaas, J., O'Dell, K., Palm, B. B., Peng, Q., Flocke, F., Pollack, I. B., Garofalo, L. A., Farmer, D. K., and Pierce, J. R.: Daytime oxidized reactive nitrogen partitioning in western US wildfire smoke plumes, Journal of Geophysical Research: Atmospheres, 126,

e2020JD033484, 2021.

Kang, S., Chen, P., Li, C., Liu, B., and Cong, Z.: Atmospheric aerosol elements over the inland Tibetan Plateau: Concentration, seasonality, and transport, Aerosol Air Quality Research, 16, 789-800, 2016.

Kang, S., Zhang, Q., Qian, Y., Ji, Z., Li, C., Cong, Z., Zhang, Y., Guo, J., Du, W., Huang, J., You, Q., Panday, A. K., Rupakheti, M., Chen, D., Gustafsson, Ö., Thiemens, M. H., and Qin, D.: Linking atmospheric pollution to cryospheric change in the Third Pole region: current progress and future prospects, National Science Review, 6, 796-809, 10.1093/nsr/nwz031, 2019.

Keck, L. and Wittmaack, K. J. A. E.: Effect of filter type and temperature on volatilisation losses from ammonium salts in aerosol matter, Atmospheric Environment, 39, 4093-4100, 2005.

Kehrwald, N. M., Thompson, L. G., Tandong, Y., Mosley-Thompson, E., Schotterer, U., Alfimov, V., Beer, J., Eikenberg, J., and Davis, M. E.: Mass loss on Himalayan glacier endangers water resources, Geophysical Research Letters, 35, 2008.

Lau, W. K., Kim, M.-K., Kim, K.-M., and Lee, W.-S.: Enhanced surface warming and accelerated snow melt in the Himalayas and Tibetan Plateau induced by absorbing aerosols, Environmental Research Letters, 5, 025204, 2010.

Lewicka-Szczebak, D., Jansen-Willems, A., Müller, C., Dyckmans, J., and Well, R.: Nitrite isotope characteristics and associated soil N transformations, Sci Rep, 11, 5008, 2021.

Li, J., Pósfai, M., Hobbs, P. V., and Buseck, P. R.: Individual aerosol particles from biomass burning in southern Africa: 2, Compositions and aging of inorganic particles, Journal of Geophysical Research: Atmospheres, 108, 2003.

Li, S. M.: Equilibrium of particle nitrite with gas phase HONO: Tropospheric measurements in the high Arctic during polar sunrise, Journal of Geophysical Research: Atmospheres, 99, 25469-25478, 1994.

Lin, Zhang, Y.-L., Yu, M., Fan, M.-Y., Xie, F., Zhang, W.-Q., Wu, G., Cong, Z., and Michalski, G.: Formation mechanisms and source apportionments of airborne nitrate aerosols at a Himalayan-Tibetan Plateau site: Insights from nitrogen and oxygen isotopic compositions, Environmental Science Technology, 55, 12261-12271, 2021.

Lin, M., Hattori, S., Wang, K., Kang, S., Thiemens, M. H., and Yoshida, N.: A complete isotope ($\delta^{15}N$, $\delta^{18}O$, $\Delta^{17}O$) investigation of atmospherically deposited nitrate in glacial-hydrologic systems across the Third Pole region, Journal of Geophysical Research: Atmospheres, 125, e2019JD031878, 2020.

Lin, W., Zhu, T., Song, Y., Zou, H., Tang, M., Tang, X., and Hu, J.: Photolysis of surface O_3 and production potential of OH radicals in the atmosphere over the Tibetan Plateau, Journal of Geophysical Research, 113, 10.1029/2007jd008831, 2008.

Lindaas, J., Pollack, I. B., Garofalo, L. A., Pothier, M. A., Farmer, D. K., Kreidenweis, S. M., Campos, T. L., Flocke, F., Weinheimer, A. J., Montzka, D. D., Tyndall, G. S., Palm, B. B., Peng, Q., Thornton, J. A., Permar, W., Wielgasz, C., Hu, L., Ottmar, R. D., Restaino, J. C., Hudak, A. T., Ku, I. T., Zhou, Y., Sive, B. C., Sullivan, A., Collett, J. L., and Fischer, E. V.: Emissions of Reactive Nitrogen From Western U.S. Wildfires During Summer 2018, Journal of Geophysical Research: Atmospheres, 126, 10.1029/2020jd032657, 2021.

Liu, X.-Y., Koba, K., Koyama, L. A., Hobbie, S. E., Weiss, M. S., Inagaki, Y., Shaver, G. R., Giblin, A. E., Hobara, S., and Nadelhoffer, K.: Nitrate is an important nitrogen source for Arctic tundra plants, Proceedings of the National Academy of Sciences, 115, 3398-3403, 2018.

Lüthi, Z., Škerlak, B., Kim, S.-W., Lauer, A., Mues, A., Rupakheti, M., and Kang, S.: Atmospheric brown clouds reach the Tibetan Plateau by crossing the Himalayas, Atmospheric Chemistry Physics, 15, 6007-6021, 2015.

Luz, B. and Barkan, E.: The isotopic ratios $^{17}O/^{16}O$ and $^{18}O/^{16}O$ in molecular oxygen and their significance in biogeochemistry, Geochimica et Cosmochimica Acta, 69, 1099-1110, 2005.

Ma, Y., Weber, R., Lee, Y. N., Orsini, D., Maxwell-Meier, K., Thornton, D., Bandy, A., Clarke, A., Blake, D., and Sachse, G.: Characteristics and influence of biosmoke on the fine-particle ionic composition measured in Asian outflow during the Transport and Chemical Evolution Over the Pacific (TRACE-P) experiment, Journal of Geophysical Research: Atmospheres, 108, 2003.

Miller, D. J., Chai, J., Guo, F., Dell, C. J., Karsten, H., and Hastings, M. G. J. G. R. L.: Isotopic composition of in situ soil NOx emissions in manure-fertilized cropland, 45, 12,058-012,066, 2018.

Ming, J., Zhang, D., Kang, S., and Tian, W.: Aerosol and fresh snow chemistry in the East Rongbuk Glacier on the northern slope of Mt. Qomolangma (Everest), Journal of Geophysical Research: Atmospheres, 112, 2007.

Morin, S., Savarino, J., Frey, M. M., Yan, N., Bekki, S., Bottenheim, J. W., and Martins, J. M.: Tracing the origin and fate of NOx in the Arctic atmosphere using stable isotopes in nitrate, Science, 322, 730-732, 10.1126/science.1161910, 2008.

Ndour, M., D'Anna, B., George, C., Ka, O., Balkanski, Y., Kleffmann, J., Stemmler, K., and Ammann, M.: Photoenhanced uptake of NO_2 on mineral dust: Laboratory experiments and model simulations, Geophysical Research Letters, 35, 2008.

Nie, W., Wang, T., Xue, L., Ding, A., Wang, X., Gao, X., Xu, Z., Yu, Y., Yuan, C., and Zhou, Z.: Asian dust storm observed at a rural mountain site in southern China: chemical evolution and heterogeneous photochemistry, Atmos. Chem. Phys., 12, 11985-11995, 2012.

Peters, B., Casciotti, K. L., Samarkin, V. A., Madigan, M. T., Schutte, C. A., and Joye, S. B.: Stable isotope analyses of NO_2^-, NO_3^-, and N_2O in the hypersaline ponds and soils of the McMurdo Dry Valleys, Antarctica, Geochimica et Cosmochimica Acta, 135, 87-101, 2014.

Pokharel, M., Guang, J., Liu, B., Kang, S., Ma, Y., Holben, B. N., Xia, X. a., Xin, J., Ram, K., Rupakheti, D., Wan, X., Wu, G., Bhattarai, H., Zhao, C., and Cong, Z.: Aerosol Properties Over Tibetan Plateau From a Decade of AERONET Measurements: Baseline, Types, and Influencing Factors, Journal of Geophysical Research: Atmospheres, 124, 13357-13374, 10.1029/2019jd031293, 2019.

Shang, X., Kang, H., Chen, Y., Abdumutallip, M., Li, L., Li, X., Fu, H., Wang, X., Wang, L., and Wang, X.: $PM_{1.0}$-nitrite heterogeneous formation demonstrated via a modified versatile aerosol concentration enrichment system coupled with ion chromatography, Environmental Science Technology, 55, 9794-9804, 2021.

Song, C. H., Park, M. E., Lee, E. J., Lee, J. H., Lee, B. K., Lee, D. S., Kim, J., Han, J. S., Moon, K. J., and Kondo, Y.: Possible particulate nitrite formation and its atmospheric implications inferred from the observations in Seoul, Korea, Atmospheric Environment, 43, 2168-2173, 10.1016/j.atmosenv.2009.01.018, 2009.

Tripathee, L., Kang, S., Rupakheti, D., Cong, Z., Zhang, Q., and Huang, J.: Chemical characteristics of soluble aerosols over the central Himalayas: insights into spatiotemporal variations and sources, Environmental Science and Pollution Research, 24, 24454-24472, 2017.

Tripathee, L., Kang, S., Chen, P., Bhattarai, H., Guo, J., Shrestha, K. L., Sharma, C. M., Sharma Ghimire, P., and Huang, J.: Water-soluble organic and inorganic nitrogen in ambient aerosols over the Himalayan middle hills: Seasonality, sources, and transport pathways, Atmospheric Research, 250, 10.1016/j.atmosres.2020.105376, 2021.

VandenBoer, T., Markovic, M., Sanders, J., Ren, X., Pusede, S., Browne, E., Cohen, R., Zhang, L., Thomas, J., and Brune, W.: Evidence for a nitrous acid (HONO) reservoir at the ground surface in

Bakersfield, CA, during CalNex 2010, Journal of Geophysical Research: Atmospheres, 119, 9093-9106, 2014a.

VandenBoer, T. C., Young, C. J., Talukdar, R. K., Markovic, M. Z., Brown, S. S., Roberts, J. M., and Murphy, J. G.: Nocturnal loss and daytime source of nitrous acid through reactive uptake and displacement, Nature Geoscience, 8, 55-60, 10.1038/ngeo2298, 2014b.

Wang, J., Zhang, Y., Zhang, C., Wang, Y., Zhou, J., Whalley, L. K., Slater, E. J., Dyson, J. E., Xu, W., Cheng, P., Han, B., Wang, L., Yu, X., Wang, Y., Woodward-Massey, R., Lin, W., Zhao, W., Zeng, L., Ma, Z., Heard, D. E., and Ye, C.: Validating HONO as an Intermediate Tracer of the External Cycling of Reactive Nitrogen in the Background Atmosphere, Environ Sci Technol, 57, 5474-5484, 10.1021/acs.est.2c06731, 2023.

Wang, K., Hattori, S., Kang, S., Lin, M., and Yoshida, N.: Isotopic constraints on the formation pathways and sources of atmospheric nitrate in the Mt. Everest region, Environmental Pollution, 267, 115274, 2020.

Wang, L., Wen, L., Xu, C., Chen, J., Wang, X., Yang, L., Wang, W., Yang, X., Sui, X., and Yao, L.: HONO and its potential source particulate nitrite at an urban site in North China during the cold season, Science of the Total Environment, 538, 93-101, 2015.

Wang, S., Liu, W., Zhao, S., Wang, C., Zhuang, L., Liu, L., Wang, W., Lu, Y., Li, F., and Zhu, G.: Denitrification is the main microbial N loss pathway on the Qinghai-Tibet Plateau above an elevation of 5000 m, Science of the total environment, 696, 133852, 2019.

Wang, Y. Q. J. M. A.: MeteoInfo: GIS software for meteorological data visualization and analysis, Meteorological Applications, 21, 360-368, 2014.

Wang, Z., Akimoto, H., and Uno, I.: Neutralization of soil aerosol and its impact on the distribution of acid rain over east Asia: Observations and model results, Journal of Geophysical Research: Atmospheres, 107, ACH 6-1-ACH 6-12, 2002.

Xu, B., Cao, J., Hansen, J., Yao, T., Joswia, D. R., Wang, N., Wu, G., Wang, M., Zhao, H., and Yang, W.: Black soot and the survival of Tibetan glaciers, Proceedings of the National Academy of Sciences, 106, 22114-22118, 2009.

Xu, J., Hettiyadura, A. P. S., Liu, Y., Zhang, X., Kang, S., and Laskin, A.: Regional differences of chemical composition and optical properties of aerosols in the Tibetan Plateau, Journal of Geophysical Research: Atmospheres, 125, e2019JD031226, 2020.

Xu, J., Zhang, X., Zhao, W., Zhai, L., Zhao, M., Shi, J., Sun, J., Liu, Y., Xie, C., Tan, Y., Li, K., Ge, X., Zhang, Q., and Kang, S.: High-resolution physicochemical dataset of atmospheric aerosols over the Tibetan Plateau and its surroundings, Earth Syst. Sci. Data Discuss., 2023, 1-45, 10.5194/essd-2023-506, 2023.

Yao, T., Thompson, L. G., Mosbrugger, V., Zhang, F., Ma, Y., Luo, T., Xu, B., Yang, X., Joswiak, D. R., and Wang, W.: Third pole environment (TPE), Environmental Development, 3, 52-64, 2012.

Ye, C., Zhou, X., Zhang, Y., Wang, Y., Wang, J., Zhang, C., Woodward-Massey, R., Cantrell, C., Mauldin, R. L., Campos, T., Hornbrook, R. S., Ortega, J., Apel, E. C., Haggerty, J., Hall, S., Ullmann, K., Weinheimer, A., Stutz, J., Karl, T., Smith, J. N., Guenther, A., and Song, S.: Synthesizing evidence for the external cycling of NOx in high- to low-NOx atmospheres, Nature Communications, 14, 10.1038/s41467-023-43866-z, 2023.

Ye, C., Zhou, X., Pu, D., Stutz, J., Festa, J., Spolaor, M., Tsai, C., Cantrell, C., Mauldin, R. L., 3rd, Campos, T., Weinheimer, A., Hornbrook, R. S., Apel, E. C., Guenther, A., Kaser, L., Yuan, B., Karl, T., Haggerty, J., Hall, S., Ullmann, K., Smith, J. N., Ortega, J., and Knote, C.: Rapid cycling of reactive nitrogen in the marine boundary layer, Nature, 532, 489-491, 10.1038/nature17195, 2016.

Yu, C., Wang, Z., Ma, Q., Xue, L., George, C., and Wang, T.: Measurement of heterogeneous uptake of NO_2 on inorganic particles, sea water and urban grime, Journal of Environmental Sciences, 106, 124-135, 2021.

Yu, W., Tian, L., Ma, Y., Xu, B., and Qu, D.: Simultaneous monitoring of stable oxygen isotope composition in water vapour and precipitation over the central Tibetan Plateau, Atmospheric Chemistry and Physics, 15, 10251-10262, 10.5194/acp-15-10251-2015, 2015.

Zhang, L., Tang, C., Huang, J., Du, T., Guan, X., Tian, P., Shi, J., Cao, X., Huang, Z., and Guo, Q.: Unexpected high absorption of atmospheric aerosols over a western Tibetan Plateau site in summer, Journal of Geophysical Research: Atmospheres, 126, e2020JD033286, 2021a.

Zhang, Y.-L., Zhang, W., Fan, M.-Y., Li, J., Fang, H., Cao, F., Lin, Y.-C., Wilkins, B. P., Liu, X., Bao, M., Hong, Y., and Michalski, G.: A diurnal story of $\Delta^{17}O(NO_3^-)$ in urban Nanjing and its implication for nitrate aerosol formation, npj Climate and Atmospheric Science, 5, 50, 10.1038/s41612-022-00273-3, 2022.

Zhang, Z., Jiang, Z., Guan, H., Liang, Y., Zheng, N., and Guo, W.: Isotopic evidence for the high contribution of wintertime photochemistry to particulate nitrate formation in Northern China, Journal of Geophysical Research: Atmospheres, 126, e2021JD035324, 2021b.

Zhang, Z., Zeng, Y., Zheng, N., Luo, L., Xiao, H., and Xiao, H.: Fossil fuel-related emissions were the major source of NH_3 pollution in urban cities of northern China in the autumn of 2017, Environmental Pollution, 113428, 2020.

Zhao, C., Yang, Y., Fan, H., Huang, J., Fu, Y., Zhang, X., Kang, S., Cong, Z., Letu, H., and Menenti, M.: Aerosol characteristics and impacts on weather and climate over the Tibetan Plateau, National Science Review, 7, 492-495, 2020.

Zhou, L., Zou, H., Ma, S., Li, P., Zhu, J., and Huo, C.: Vertical air mass exchange driven by the local circulation on the northern slope of Mount Everest, Advances in Atmospheric Sciences, 28, 217-222, 2011.

Zhou, T., Jiang, Z., Zhou, J., Zhao, W., Wu, Y., Yu, H., Li, W., Zhang, Z., Su, G., Ma, T., and Geng, L.: Fast and Efficient Atmospheric NO_2 Collection for Isotopic Analysis by a 3D-Printed Denuder System, Anal Chem, 94, 13215-13222, 10.1021/acs.analchem.2c02839, 2022.

Zhu, T., Lin, W., Song, Y., Cai, X., Zou, H., Kang, L., Zhou, L., and Akimoto, H.: Downward transport of ozone-rich air near Mt. Everest, Geophysical Research Letters, 33, 2006.

Zong, Z., Sun, Z., Xiao, L., Tian, C., Liu, J., Sha, Q., Li, J., Fang, Y., Zheng, J., and Zhang, G.: Insight into the Variability of the Nitrogen Isotope Composition of Vehicular NOx in China, Environ. Sci. Tech., 54, 14246-14253, 10.1021/acs.est.0c04749, 2020.

Zou, H., Zhou, L., Ma, S., Li, P., Wang, W., Li, A., Jia, J., and Gao, D.: Local wind system in the Rongbuk Valley on the northern slope of Mt. Everest, Geophysical Research Letters, 35, https://doi.org/10.1029/2008GL033466, 2008.

Uncategorized References

Cardoso, J., Almeida, S. M., Nunes, T., Almeida-Silva, M., Cerqueira, M., Alves, C., Rocha, F., Chaves, P., Reis, M., and Salvador, P.: Source apportionment of atmospheric aerosol in a marine dusty environment by ionic/composition mass balance (IMB), Atmospheric Chemistry and Physics, 18, 13215-13230, 2018.

Chen, L., Peng, C., Gu, W., Fu, H., Jian, X., Zhang, H., Zhang, G., Zhu, J., Wang, X., and Tang, M.: On mineral dust aerosol hygroscopicity, Atmospheric Chemistry and Physics, 20, 13611-13626, 2020.

Engelbrecht, J. P., Moosmüller, H., Pincock, S., Jayanty, R., Lersch, T., and Casuccio, G.: Mineralogical,

chemical, morphological, and optical interrelationships of mineral dust re-suspensions, Atmospheric Chemistry and Physics, 16, 10809-10830, 2016.

Fang, T., Guo, H., Verma, V., Peltier, R., and Weber, R.: PM 2.5 water-soluble elements in the southeastern United States: automated analytical method development, spatiotemporal distributions, source apportionment, and implications for heath studies, Atmospheric Chemistry and Physics, 15, 11667-11682, 2015.

Gao, Q., Zhu, S., Zhou, K., Zhai, J., Chen, S., Wang, Q., Wang, S., Han, J., Lu, X., and Chen, H.: High enrichment of heavy metals in fine particulate matter through dust aerosol generation, Atmospheric Chemistry and Physics, 23, 13049-13060, 2023.

Liu, B., Cong, Z., Wang, Y., Xin, J., Wan, X., Pan, Y., Liu, Z., Wang, Y., Zhang, G., Wang, Z., Wang, Y., and Kang, S.: Background aerosol over the Himalayas and Tibetan Plateau: observed characteristics of aerosol mass loading, Atmospheric Chemistry and Physics, 17, 449-463, 10.5194/acp-17-449-2017, 2017.

Long, H., Cheng, L., Yang, F., and Zhang, G.: Temperature regulates dust activities over the Tibetan Plateau, The Innovation, 6, 2025.

Ma, Y., Xie, Z., Ma, W., Han, C., Sun, F., Sun, G., Liu, L., Lai, Y., Wang, B., and Liu, X.: QOMS: a comprehensive observation station for climate change research on the top of Earth, Bulletin of the American Meteorological Society, 104, E563-E584, 2023.

Matsumoto, K., Minami, H., Uyama, Y., and Uematsu, M.: Size partitioning of particulate inorganic nitrogen species between the fine and coarse mode ranges and its implication to their deposition on the surface ocean, Atmospheric Environment, 43, 4259-4265, 2009.

Seisel, S., Lian, Y., Keil, T., Trukhin, M. E., and Zellner, R.: Kinetics of the interaction of water vapour with mineral dust and soot surfaces at T= 298 K, Physical Chemistry Chemical Physics, 6, 1926-1932, 2004.

Tang, M., Cziczo, D. J., and Grassian, V. H.: Interactions of Water with Mineral Dust Aerosol: Water Adsorption, Hygroscopicity, Cloud Condensation, and Ice Nucleation, Chemical Reviews, 116, 4205-4259, 10.1021/acs.chemrev.5b00529, 2016.

Tang, M., Zhang, H., Gu, W., Gao, J., Jian, X., Shi, G., Zhu, B., Xie, L., Guo, L., and Gao, X.: Hygroscopic properties of saline mineral dust from different regions in China: Geographical variations, compositional dependence, and atmospheric implications, Journal of Geophysical Research: Atmospheres, 124, 10844-10857, 2019.

Vicars, W. C. and Savarino, J.: Quantitative constraints on the ^{17}O-excess ($\Delta^{17}O$) signature of surface ozone: Ambient measurements from 50°N to 50°S using the nitrite-coated filter technique, Geochimica et Cosmochimica Acta, 135, 270-287, 10.1016/j.gca.2014.03.023, 2014.

Wang, F., Ge, W., Luo, H., Seo, J.-H., and Michalski, G.: Oxygen-17 anomaly in soil nitrate: A new precipitation proxy for desert landscapes, Earth and Planetary Science Letters, 438, 103-111, 2016.

Wu, F., Zhang, D., Cao, J., Xu, H., and An, Z.: Soil-derived sulfate in atmospheric dust particles at Taklimakan desert, Geophysical research letters, 39, 2012.

Wu, F., Cheng, Y., Hu, T., Song, N., Zhang, F., Shi, Z., Hang Ho, S. S., Cao, J., and Zhang, D.: Saltation–sandblasting processes driving enrichment of water-soluble salts in mineral dust, Environmental Science & Technology Letters, 9, 921-928, 2022.

Xuan, H., Liu, C., Zhang, P., Chu, B., Liang, L., Ma, Q., and He, H.: A Review of Laboratory Studies on the Heterogeneous Chemistry of NO2: Mechanisms and Uptake Kinetics, The Journal of Physical Chemistry A, 2025.

994 Zhang, Z., Zhou, T., Jiang, Z., Ma, T., Su, G., Ruan, X., Wu, Y., Cao, Y., Wang, X., Liu, Z., Li, W., Zhang,
995 H., Lin, M., Liu, P., and Geng, L.: High-Resolution Measurements of Multi-Isotopic Signatures (δ15N,
996 δ18O, and Δ17O) of Winter NO2 in a Megacity in Central China, Environmental Science & Technology,
997 59, 3634-3644, 10.1021/acs.est.4c07724, 2025.

998